Charles University

Faculty of Science

Study program: Chemistry

Branch of study: Chemistry

Branislav Koreň

Synthesis and characterization of UZM-9 zeolite

Bachelor’s thesis

Supervisor:

Ing. Martin Kubů, Ph.D.

Prague, 2024

Univerzita Karlova

Přírodovědecká fakulta

Studijní program: Chemie

Odvětví studia: Chemie

Branislav Koreň

Syntéza a charakterizace zeolitu UZM-9

Bakalářská práce

Školitel:

Ing. Martin Kubů, Ph.D.

Praha, 2024

Prohlášení

Prohlašuji, že jsem závěrečnou práci zpracoval samostatně a že jsem uvedl všechny použité informační zdroje a literaturu. Tato práce ani její podstatná část nebyla předložena k získání jiného nebo stejného akademického titulu.

Jsem si vědom toho, že případné využití výsledků, získaných v této práci, mimo Univerzitu Karlovu je možné pouze po písemném souhlasu této univerzity.

V Praze dne 23.5.2024

Acknowledgement

I would like to thank my supervisor Ing. Martin Kubů, Ph.D., my consultant Prof. Ing. Jiří Čejka DrSc., and his research group for their time, guidance, and patience during my research. Furthermore, I would like to thank them for the help with the experiments and sample measurements. Finally, I would like to express my gratitude to Euro Support Manufacturing Czechia, s.r.o for their financial support of my research.

Abstract

UZM-9 zeolite of LTA framework holds significant importance due to its unique structure and properties, making it suitable for various industrial processes such as gas separation, ion exchange, and catalysis. Optimizing the synthesis process is crucial to enhance its performance and applicability. This research aims to contribute to develop efficient and cost-effective methods for its production, furthering its potential in industrial applications.

The main objectives include the optimization of synthesis parameters, isomorphous substitution, and adsorption studies. Optimization involved the addition of seeding crystals, reducing structure-directing agents, and selecting reactant sources. Direct synthesis of Fe and Zr forms of the UZM-9 zeolite by isomorphous substitution was studied. Adsorption studies examined CO_2 on different cation forms, while the texture properties were studied by nitrogen adsorption. Prepared zeolites were further characterised by XRPD, SEM, ICP-MS, and FT-IR.

Results show significantly improved crystallization times, enhanced texture properties, and the effects of using various sources of reactants. Isomorphous substitution of Fe atoms was unsuccessful, while showing promising results for Zr. Various ion-exchanged forms of UZM-9 zeolite were shown to have their adsorption properties affected by the cations present in their pores, while the results also varied with adsorbed gas.

Overall, the study managed to optimise the synthesis, possibly making it economically viable, while thoroughly researching its characteristics and therefore possibilities of its utilization.

Key words: UZM-9 zeolite, LTA, synthesis, adsorption, CO_2

Abstrakt

Zeolit UZM-9 s mřížkou LTA je významný díky své jedinečné struktuře a vlastnostem, které jej činí vhodným pro různé průmyslové procesy, jako jsou separace plynů, iontová výměna a katalýza. Optimalizace syntézního procesu je klíčová pro zvýšení jeho využitelnosti v průmyslových procesech. Tento výzkum si klade za cíl přispět k vývoji účinných a nákladově efektivních metod jeho výroby, čímž se rozšíří jeho potenciál v průmyslových využitích.

Hlavní cíle zahrnují optimalizaci syntézních parametrů, izomorfní substituci a studia adsorpce. Optimalizace spočívala v přidání očkovacích krystalů, snížení množství organického templátu a výběru zdrojů reaktantů. Byla také zkoumána přímá syntéza Fe a Zr forem zeolitu UZM-9 pomocí izomorfní substituce. Adsorpční studie zkoumaly adsorpci CO_2 v různých kationtových formách, zatímco texturní vlastnosti byly zkoumány pomocí adsorpce dusíku. Připravené zeolity byly dále charakterizovány pomocí XRPD, SEM, ICP-MS a FT-IR.

Výsledky vykazují výrazně nižší časy krystalizace, vylepšené texturní vlastnosti a vliv použití různých zdrojů reaktantů. Izomorfní substituce Fe atomů byla neúspěšná, zatímco se Zr atomy poskytla slibné výsledky. Různé formy zeolitu UZM-9 s vyměněnými ionty prokázaly, že jejich adsorpční vlastnosti jsou ovlivněny kationty přítomnými v jejich pórech, přičemž se výsledky lišily i v závislosti na adsorbovaném plynu.

Celkově se studii podařilo optimalizovat syntézu zeolitu UZM-9, čímž jej potenciálně učinila ekonomicky výhodným. Také důkladně prozkoumala jeho vlastnosti, a tedy i možnosti jeho využití.

Klíčová slova: UZM-9 zeolit, LTA, syntéza, adsorpce, CO_2

Table of contents

List of abbreviations

BET	Brunauer–Emmett–Teller
CBU	Composite building units
CDM	Charge density mismatch
CSA	Chemical shift anisotropy
DEDMAOH	Diethyldimethylammonium hydroxide
FCC	Fluid catalytic cracking
FID	Free induction decay
FT-IR	Fourier transform infrared spectroscopy
GAC	Granular activated carbons
ICP-MS	Inductively coupled plasma mass spectrometry
IZA	International Zeolite Association
NMR	Nuclear Magnetic Resonance
SDA	Structure Directing Agent
SBU	Secondary building units
SEM	Scanning electron microscopy
TBU	Tetrahedral building unit
TEACl	Tetramethylammonium chloride
TEAOH	Tetramethylammonium hydroxide
TMAOH	Tetramethylammonium hydroxide
XRD	X-Ray Diffraction
XRPD	X-Ray powder diffraction

Aims of the thesis

The thesis will be focused on the synthesis and characterisation of UZM-9 zeolite with LTA topology to accomplish following goals

- optimization of the synthesis by addition of seeding crystals, lowering amounts of SDAs, and the most optimal reactant sources
- direct synthesis of Fe and Zr form of UZM-9 zeolite by isomorphous substitution
- understanding CO_2 adsorption on sodium, lithium, and potassium forms of UZM-9 zeolite

1 Theoretical part

1.1. Zeolites

1.1.1. History and use

Zeolites were first described in 1756 by Axel F. Cronstedt, who found them in Sweden and Iceland. Their name comes from the Greek words zeo (to boil) and lithos (stone) as they seem to boil when heated. Since 1756, there were many discoveries of different kinds of natural zeolites and their properties, such as the ability to adsorb and desorb water without change in their morphology, as described by A. Damour in 1857.[1] It was later shown that zeolites after being dehydrated are also capable of adsorbing various gasses, such as carbon dioxide, hydrogen sulphide, chloroform, ammonia etc.[2] Dehydrated chabazite was also shown to adsorb ammonia, but not benzene or diethyl ether, described by J. W. McBain.[3]

The first zeolite was synthesised in 1862 by H. Saint-Claire-Deville[4] using hydrothermal synthesis, but it was possible to characterise and therefore acknowledge synthesis of new synthetic zeolites only in 1940s, after the development of XRD techniques suitable for polycrystalline material characterisation. The first such zeolites were named P and Q. They did not have any natural counterparts. Development of new zeolites continued mostly in industry and at the beginning, it was not met with understanding of possibilities that zeolites provide. First patents were published in late 1950s and the syntheses used only inorganic molecules. First zeolites were used as adsorbents and also for separation and purification.[5] The first time, when the quaternary ammonium cations (TMAOH) were used as structure directing agents (SDA) was in 1961 by R.M. Barrer and P.J. Denny, during synthesis of zeolites Y, A and X.[6] Zeolite Beta and ZSM-5 were the next important materials, being prepared with the addition of TEAOH and TPAOH, respectively. The variability of SDAs and their use in zeolite synthesis have spurred new research, leading to the discovery of novel structures with diverse pore systems and frameworks. As a result, the International Zeolite Association (IZA) has currently approved 256 distinct structures.[7]

Zeolites have found applications as catalysts in oil refining and petrochemical industry, adsorption, separation, and ion exchange with other research areas still being explored.[8] Reactants in heterogeneous catalysis are in a different phase than catalyst, being mostly in solid phase, while reactants tend to be fluids. The process of heterogeneous catalysis consists of diffusion of liquid or gaseous reactant mixture into catalyst, adsorption, chemical reaction, and

desorption, leading to regeneration of catalytic site. Performance of catalyst can be attributed to four main areas, its activity, selectivity for desired product, stability and regenerability.[9] Zeolites and other solid catalysts replaced homogeneous catalysts as they surpass them in many areas, such as regeneration, separation from reactants, stability, and lowered negative environmental impact. The specific advantages of zeolites, contribute to their applications as catalysts in oil refining, petrochemical industries, adsorption, separation, and ion exchange, with ongoing exploration into additional research areas. These advantages arise from the coordination of different heteroatoms within the zeolite structures. For example, trivalent heteroatoms like aluminium can act as Lewis acid sites due to their free orbitals, which can accept electron pairs. On the other hand, Brønsted acid sites are formed when the negative framework charges of the zeolite are balanced by protons, making these sites capable of donating protons. Thus, the zeolite framework supports both Lewis and Brønsted acid sites, enhancing its catalytic properties.[10] Porosity and large surface areas with many active sites inside the pores are desirable properties of zeolites, but those are also present in other porous materials. However, the specific characteristic of zeolites comes from their uniform pore openings, which provide possibilities of shape selectivity. It can be based on molecules of suitable shapes being capable of entering the pores of the zeolite (reactant selectivity), possibility of forming the transition state and subsequently products inside of the pores (transition state selectivity) and their ability to leave pores (product selectivity).[8] Acid catalyst properties of zeolites are one of the most commercially used ones, with implementation mostly in petrochemical industry, in processes such as fluid catalytic cracking (FCC).

Adsorption is used for separation of chemicals mostly when other, more used, and available, processes fail because of their properties or economic viability. It is based on different affinity for adsorption onto a surface of adsorbent by separated chemicals. For example, this makes them capable of separation based on affinity to water influenced by their polarity that arises from different Si/Al ratio. Cations within the pores also affect their polarizability. Zeolites provide another advantage which stems from the ability to tune their pore sizes and composition. The shape selectivity of zeolite enables them to act as molecular sieves, separating desired chemicals based on both their dimensions and their adsorption properties. The examples include separation of hydrocarbons with similar physicochemical properties, such as separation of p-xylene from xylene mixture by ZSM-5 zeolite[11] or ethane and ethylene by zeolites with LTA framework.[12,13] The almost infinite reversibility of adsorption and desorption of molecules, makes them so feasible for commercial use in gas treatment,

production of fine chemicals, and pharmaceutical industry. Zeolites also show benefits in environmental protection, specifically wastewater treatment and their capability of filling the gaps that are left by granular activated carbons (GAC), such as removal of highly soluble and polar chemicals.[8]

The low cost of manufacturing and negligible environmental impact, make ion exchanged zeolites the most produced synthetic zeolites. Na^+ containing zeolite A is the most common one, being able to easily exchange its cations with Ca^{2+} or Mg^{2+} from water, which makes it part of almost every detergent, therefore making it the most produced synthetic zeolite in the world.[8]

1.1.2. Structure and properties

Zeolites are defined as microporous crystalline aluminosilicate materials consisting primarily of TO_4 tetrahedra crosslinked through O-bridges. Present T atoms are traditionally Si or Al, but it is possible to exchange them with other atoms such as B, P, Ge, etc. Their simplified formula is

$$M^{n+}_{x/n}Al_xSi_{1-x}O_2 \cdot yX,$$

where x is between 0 and 0.5, M^{n+} represents the cation, and X neutral molecules in the pores. Even though Si/Al ratios in zeolites differ, they are never below 1, as explained by Lowenstein rule, since connection between two aluminium atoms is forbidden.[10] It is the arrangement of tetrahedra that determines framework of zeolites, which is a source of their properties. They are microporous materials defined by their cavities and pore systems, which give them their designation as molecular sieves. Understanding of frameworks composition, their pore systems, and density provides knowledge about functionality of zeolites, since they influence their catalytic, adsorption, and ion-exchange capabilities.[14,15]

Zeolites can be described by their building units, with TO_4 tetrahedra being the primary ones. However, the building units of higher order such as secondary building units (SBU), composite building units (CBU), and natural building units (NBU) were devised to better describe the zeolite structures. SBU's are the smallest possible topological entities, which are capable of forming whole zeolite framework, while only using one of the 23 known ones. However, this idea has now been rejected by discovery of new and more complex zeolites that

need at least 2 SBUs.

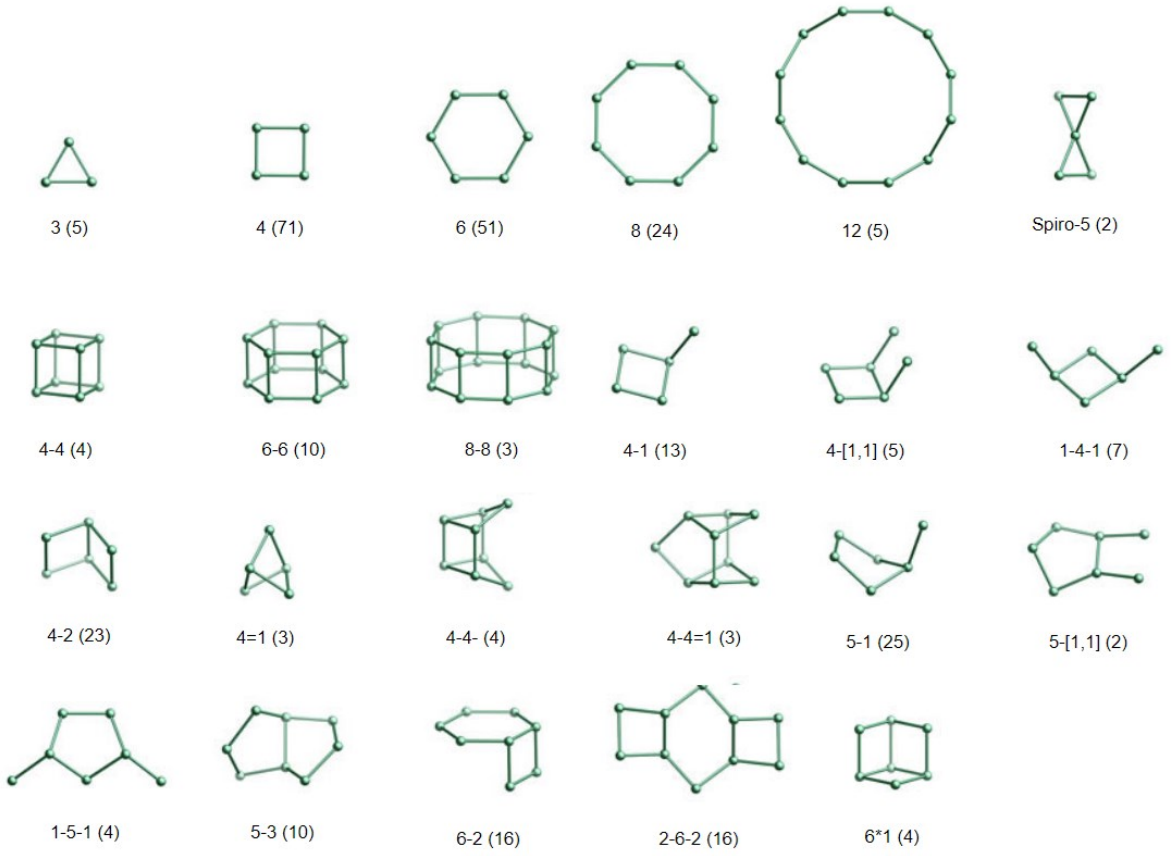

Figure 1: Secondary building units (SBU) of zeolites[16]

CBUs were found to be even better suited for zeolite description as they represent common substructures of zeolites such as cages, links, chains, and channels. They are represented in various zeolites and show their common themes and relationships. The NBUs, or natural tiles, were assigned to zeolites to solve issues of ambiguity that came with SBUs and CBUs. Their advantages are in their unambiguity as they fill the whole crystal space, and they enumerate all minimal cavities and windows in system.[14]

Channel systems of zeolites depend on the sizes of the pore openings, which can be considered small, if they contain 8-ring of T atoms. Medium ones have 10-rings and large ones have 12-rings with anything larger than that being considered extra-large. Those channels are cylindrical and can have either regular or elliptical shape with possibilities of intersections creating cages and cavities with windows. Channels can be arranged into 1, 2 or 3 dimensional systems, based on their interconnection.[14, 15]

Framework types of zeolites are designated by three letter codes that were assigned to them based on the name of zeolite or the type of material they were based on. For example,

materials with same framework topology as natural faujasite, have been assigned the code FAU, while LTA code comes from the name of zeolite Linde Type A. Differentiation from framework structures is also necessary as the framework types describe topology of zeolites and only the interconnectivity between the T atoms in the most symmetrical way. On the other hand, the zeolite structure covers the composition of the materials, including arrangement of the T atoms, presence of extra-framework atoms, molecules in pores and various deformations of material, which means that different zeolite structures may share the same framework type. Many different heteroatoms may be present in the zeolite structure, as they are interchangeable with Al, resulting in immense effect on its properties. Possibilities of different compositions vary not only with heteroatoms but also their Si/Al ratios. Si/Al ratio of zeolite ranges from high silica (Si/Al > 12), which have tendency to form 5-rings, to high alumina ($1.2 \leq Si/Al \leq 3.0$).

Extra-framework species, such as Li^+, Na^+, K^+, etc., present in the pores, are of significant importance as they provide zeolites with properties necessary for ion exchange, catalysis, and adsorption. Their position in zeolite framework is specific for each framework structure.[14,17]

UZM-9 zeolite has LTA topology with its as synthesized form having Si/Al ratios between 3.5 – 6.[18] LTA topology named after Linde type A material is a small pore zeolite with three-dimensional channel system composed of straight channels with α-cavities, at its intersection. The framework is composed of *d4r*, *sod*, and *lta* CBUs as shown in Figure *2*. Ring size of *lta* units are 8 membered with the size 4.1 Å in diameter but extra-framework cations can influence its sizes.

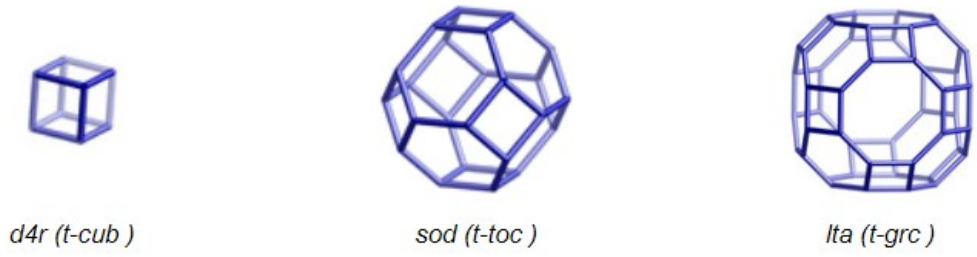

Figure 2: CBUs of LTA framework type[19]

Its framework density is 14.2 T-atoms per 1000 $Å^3$, which is considered to be very open and therefore capable of adsorbing large amounts of substances. Si/Al ratio is the main difference between UZM-9 (Si/Al = 3-6) and typical LTA species such as zeolite A (Si/Al = 1) or zeolite NaA. [19,14]

1.1.3. Structure directing agents

Structure directing agents (SDA) are organic molecules used in hydrothermal syntheses to prepare new zeolite structures by organising inorganic precursors and influence crystallization process towards a desired product. This influence is based on their shape, size, hydrophilicity/hydrophobicity, rigidity, and stability in hydrothermal syntheses. Their role may be described by their structure directing and pore filling effect. Those affect the structure based on their size and shape, crystallization of framework type not observed without their presence, and stabilization of open pore system respectively.[20] The use of SDAs allowed synthesis of zeolites with lower aluminium contents, since the large organic molecules compensate lower amount of negatively charged of trivalent heteroatoms, than the inorganic ions, so the Al atoms aren't incorporated into framework as much. Although, as shown, SDAs are not always specific enough, so their use does not lead to one desired product, as specific synthesis conditions are necessary. This means, in specific situations, that it is possible to obtain many different zeolite structures from one SDA, but the use of various SDAs can lead to the same structure. Quaternary ammonium cations are the most used SDAs, but other amines, oxygenates, or quaternary phosphonium cations were investigated and used. It was found by Y. Kubota et al.[21], that the best ratio of C/N^+ is between 11-16, as it provides moderate hydrophobicity which makes crystallization easier.[22]

1.1.4. Synthesis

Finding the proper conditions for synthesizing the aluminosilicate structure of zeolites with desired properties has been a challenge since the discovery of the first synthetic zeolite. Syntheses are influenced by many factors, such as composition of synthesis mixture and its pH, crystallization time, the presence of various mineralizing agents, the amount of water, the homogeneity of the mixture, temperature, SDAs etc.[22]

Hydrothermal synthesis is the most common way of synthesizing zeolites, performed under aqueous conditions, under agitation or static conditions, and usually at elevated temperatures. Choosing proper sources of silica and alumina is necessary, as silica source affects final products due to different particle sizes of the sources, influencing solution pH, reactivity, solubility, and the ability to stir the mixture. Alumina sources also affect pH of solution as they can be neutral, alkaline, or acidic.[22]

Basic conditions are desirable during synthesis as they provide environment for easier dissolution of reactants and also allows homogenization and formation of oxygen bridges

between framework atoms. Presence of hydroxide ions in lower amounts results in difficult dissolution of reagents, while their excess results in phases that are too dense and undesired. Factors such as the Si/Al ratio, the rate of crystallization, and crystal sizes may be also influenced by amount of OH^- ions. This allows possibility of synthesising various zeolites by changing only the hydroxide amounts in synthesis mixture exemplified in refferences[23,24], where the increase of $NaOH/SiO_2$ ratio changed the products from amorphous phase, through ZSM-5, until resulting in mordenite and analcime. Another factor to consider is the source of hydroxides, commonly sodium hydroxide (NaOH) or potassium hydroxide (KOH), as the difference in cation sizes influences the final product through their interactions with framework, since the sodium cations prefer 6-ring tetrahedral building units (TBU), while potassium cations prefer 8-ring TBUs. Mixing the aforementioned reagents results in formation of precursor network of various structures. The Si/Al ratio is one of the primary determinants of structure that will be formed, as it can result in formations of different structures even while rest of the composition of the mixture stays the same. Lower ratios ($Si/Al \leq 5$) produce 4, 6 and 8 membered rings while formation of 5 membered rings becomes more common with an increase in the Si/Al ratio. Water is the most commonly used solvent in syntheses, as the non-aqueous solvents have shown to be worse at solubilising the synthesis mixture and can prolong the crystallization times. It has effect on viscosity, as lowering the amount of water in mixture results in formation of slurry, wet paste or gel with various levels of dryness that affect homogenization. Additionally, water serves as mediator of condensation reaction between the silica and alumina species during the growth of crystals. Subjecting the precursor mixture to increased temperatures results in increase of rate at which the precursor phases start to dissolve and begin to form nucleation sites with different structures. Si and Al atoms from solution then migrate to crystal nuclei, when the structure of nucleation site from the initial stage of synthesis reaches the one suitable for further crystal growth.[22]

1.1.5. Experimental charge density matching approach

An experimental charge density matching approach to zeolite synthesis involves the initial formation of CDM (Charge Density Mismatch) in the precursor mixture, which is a result of using a large, low-density SDA and a high-density aluminosilicate network, with a low Si/Al ratio, thus creating mismatch in their charge densities. Hydroxide levels and temperature also influence these mixtures.[25] CDM is created as a result of these factors, making it very difficult or even impossible for the precursor aluminosilicate network to form, allowing the development of different precursors that can lead to new crystalline structures. This approach allows use

of large SDA and low Si/Al ratio of the mixture, with its advantage being in greater control of the crystallization process and also cooperation of various templates. Only the addition of another SDA molecule, which is smaller and has a more suitable charge density match, induces crystallization.[25, 26] The preparation of UZM-9 zeolite according to this approach involves using a mixture of organic cations, in which at least one has an organic group with a number of carbons larger than one (such as the ethyl group in TEA^+ or $DEDMA^+$).[18] Supplementary SDAs that match the charge density of the mixture used in these syntheses can be small inorganic cations such as sodium or potassium, or small organoammonium molecules such as TMA^+.[26]

1.2. Characterisation methods

1.2.1. X-ray diffraction

The X-ray diffraction (XRD) technique is one of the most familiar, effective, and non-destructive methods used in the characterization of crystalline structures. It is used to obtain many characteristics of the studied material, such as its phases, texture, and crystallinity. This method is named after X-rays, which have energy that corresponds to wavelengths matching interatomic distances in solid materials. Monochromatic X-ray beams necessary for this technique are created in a process where electrons are released from a heated filament. These electrons are then accelerated onto a target material, with copper being the most commonly used one, where they hit inner shell electrons, resulting in the release of X-rays. These are then filtered and allowed to fall onto a sample as monochromatic beams. The diffraction of these beams on atoms of the sample results in the interference of scattered waves, which then create distinctive XRD patterns of peaks specific to each individual material. The basic principle of XRD is expressed by Bragg's equation:

$$n\lambda = 2d\sin\theta, \qquad 1$$

where n is order of diffraction, λ is wavelength of X-rays, d is interplanar distance and θ is angle of beam that falls and scatters from atomic planes. Knowledge of X-ray wavelengths and θ from experiment then allows us to calculate interplanar distance d of studied material.[27]

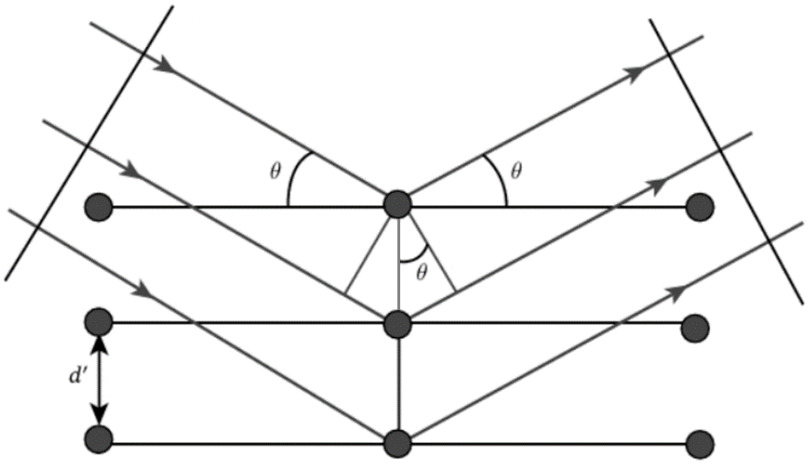

Figure 3: Diffraction of X-rays[27]

Characterisation of crystalline materials in their powder form is done by X-ray powder diffraction (XRPD). It is great for distinguishing between amorphous, crystalline or the mixed forms of the studied material, since its diffractograms show diffraction lines corresponding ordered structure of crystalline materials, while amorphous phases, lacking ordered lattices, show diffuse patterns. The main uses of XRPD include evaluating degree of crystallinity, differentiation of various crystals, and showing phase transformation differences.[28] Patterns obtained from this technique are primarily used as fingerprints for identifying specific crystalline materials, as there are libraries of known XRPD diffractograms available for comparison. It is also possible to obtain information about their properties coming from shapes, intensities, and distribution of peaks.

Powder diffraction pattern in zeolites contains all aforementioned information. Positions of peaks, measured in 2θ, correspond to reflection positions of X-rays, which are a result of lattice spacing. Intensity of peaks is a result of summation of all the detected X-ray reflection at given angle, which means they are related to composition of sample and its crystal structure. Another information comes from peak width showing crystal quality as wider peaks mean that cell parameters are not as well-defined, although they may be influenced by other factors such as crystallite size or intrinsic instrumental peak width. It is also necessary to consider the background of diffractogram, as it may indicate presence of amorphous phases or other impurities.[26]

1.2.2. Scanning electron microscopy

Scanning electron microscopy (SEM) uses a finely focused probe electron beam, typically ranging from a few hundred eV to tens of keV, to scan the studied material. Interactions of electrons with the solid surface produce various responses, including secondary electron emission. The intensity of emitted electrons varies based on the angle of impact of the probe electrons and the surface topography, resulting in SEM images that display different brightness levels corresponding to varying secondary electron intensities detected by SEM sensors.[29]

1.2.3. Gas adsorption

Gas adsorption plays an important role in characterisation of zeolites and other porous materials to study their surface areas, porosity, and pore volume, which are crucial characteristics considering their utilization. Adsorption is a phenomenon where fluids interact with solids, leading to an increase in density as they approach the solid boundary. Conversely, desorption is the reverse process, where fluids are released from the solid surface, resulting in a decrease in density. Physisorption and chemisorption are two types of adsorption, differing in type of interactions between the solid and fluid. Van der Waals forces are typical for physisorption while the molecules of fluid chemically bond to solid surface in chemisorption. Low temperatures are required for physisorption due to its weak interactions, but this weakness also allows the process to be reversible. Adsorption measurements are mostly presented as isotherms, which show dependence of the adsorbed gas amount on partial pressure at constant temperature. Based on IUPAC classification there are eight general types of isotherm, as shown on Figure 4, which are a specific to different materials.[30] Isotherm specific for zeolites and other microporous materials is the type I, which corresponds to Langmuir theory and shows fast monolayer formation and subsequent saturation.[31]

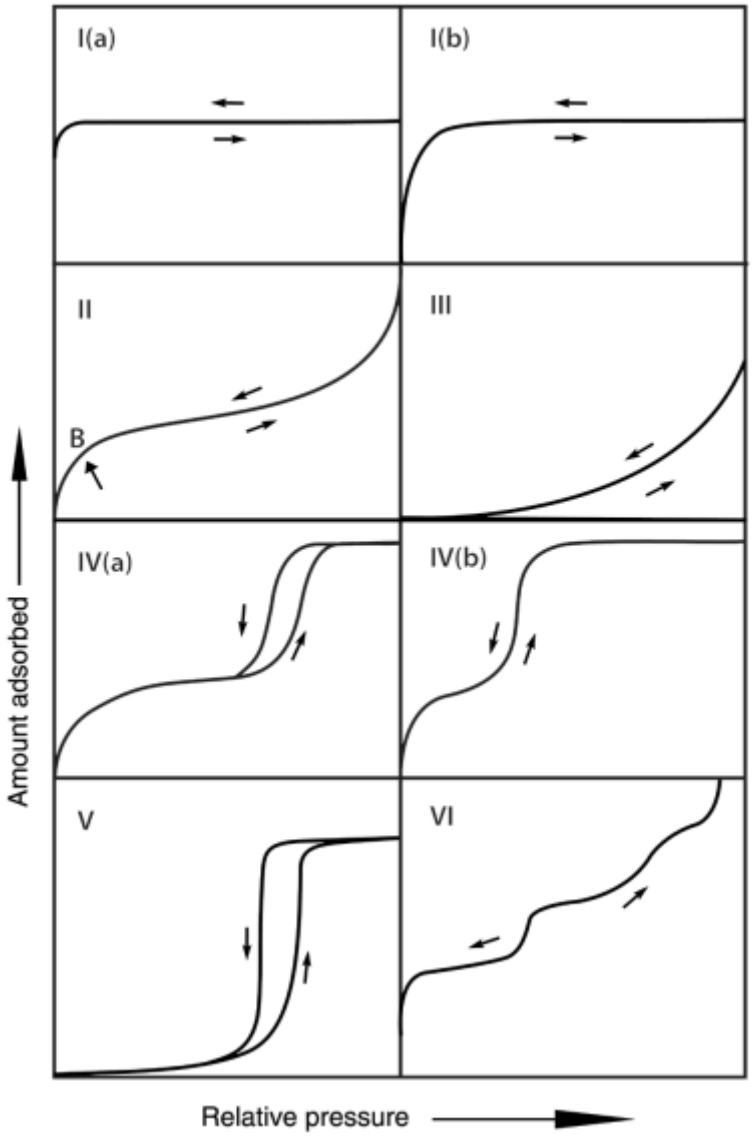

Figure 4: Main types of gas physisorption isotherms[32,33]

Measurements of adsorption isotherms are most typically done by using nitrogen as probe molecule at temperature of -196 °C (its boiling temperature), but other gases such as argon at -186 °C (liquid argon temperature) or carbon dioxide at 0 °C are used.[32] The temperature for CO_2 is chosen as it is relevant for applications such as carbon capture and storage. Calculations are mostly done using Langmuir theorem, which operates only with monolayer of adsorbed gas, or BET (Brunauer–Emmett–Teller) theorem, an advancement of former theory, which incorporates possibility of more layers. [31,34]

1.2.4. Solid-state nuclear magnetic resonance

Nuclear magnetic resonance (NMR) measurements arise from intrinsic angular momentum, also called spin, which is a quantum mechanical property possessed by nuclei.[35] Spin is

a quantized value represented by vectors. It gives rise to magnetic moments which are directly proportional to this property, as shown by Equation 2

$$\vec{\mu} = \gamma \cdot \vec{S}, \quad 2$$

where $\vec{\mu}$ represents magnetic moment, γ is magnetogyric ratio and $\vec{S}$ is spin. Spin produces angular momentum which has discrete values because of its quantization. They correspond to levels in magnetic field B_0 and their energy is determined by Zeeman interaction. This interaction depends on magnetic moment, which is dependent on spin and magnetic field as shown by Equation 3.

$$E = -\vec{\mu} \cdot \vec{B} \quad 3$$

As a result, it is possible to observe energy of nuclear spin splitting into energetic levels based on the value of the spin. Application of weakly oscillating magnetic field, with energy corresponding to distance between those energy levels in the magnetic field, results in production of signal from resonating nucleus. Nowadays, the procedure goes as follows: a short pulse with radio frequency excites the nuclei, resulting in free induction decay (FID), which can be observed by sensors. Fourier transformation of FID produces NMR spectra which show dependence of intensity on how different surroundings affect nuclei in magnetic field with known frequency.[35]

Main framework atoms of zeolites are elements with NMR active nuclei ^{27}Al and ^{29}Si. This allows characterisation of zeolites by solid state NMR as it provides information about local surrounding of those atoms and therefore structure of the material. However, those measurements are met with difficulties, which rise from their solid state. Nuclei having anisotropic interactions with their local environment results in the broadening of NMR signals. Other sources of the line broadening are dipole-dipole interactions between neighbouring nuclei and chemical shift anisotropy (CSA), which is a result of spatial dependence of electron shielding. Another reason may be quadrupole interaction, which is the case for nuclei with spin number larger than ½, such as ^{27}Al. Although, those interactions cause lower resolution of NMR spectra, they may also be used as a source of information such as intermolecular distances and geometries, coordination symmetry and charge distribution around nucleus, respectively.[35,36]

To solve aforementioned issues and to measure high resolution NMR spectra, it was necessary to develop line narrowing procedures such as magic angle spinning (MAS) and cross polarization experiments. MAS experiment is used for removal of negative effects of CSA and

dipolar interactions in solid samples. It is based on the fact, that effects of those line broadening interactions have similar angle dependence in form of $3\cos^2\theta - 1$. By spinning the sample at high frequencies and under the angle $\theta = 54.736°$ (magic angle) with respect to magnetic field B_0, those interactions average to zero, resulting in significant increase in resolution of the NMR spectrum. This is achieved by packing the sample into the rotor, which tends to be made of zirconia and is being spun in a probe with dry air or nitrogen as bearing as shown in Figure 5.

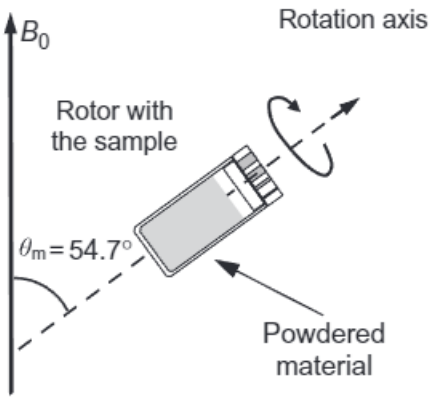

Figure 5: Scheme of MAS technique[35]

Cross polarization experiment increases sensitivity of a nucleus with low abundance, for example ^{29}Si in zeolites, by transferring magnetization from abundant nucleus. Nucleus used as an abundant source of magnetization is most often ^{1}H. Experiment starts with excitation of the abundant nucleus, magnetization transfer to less abundant nucleus, and ends with acquisition of FID. Cross polarization is useful in shortening experiment times, since ^{1}H nucleus has much shorter relaxation time than ^{29}Si. Another use is in the structure determination by considering relative intensities of peaks. This happens because of the cross polarization mechanism, which happens through dipolar coupling, so the nuclei of ^{29}Si, that are closer to ^{1}H, have higher intensities.[35, 37]

1.2.5. Fourier-transform infrared spectroscopy

Infrared spectroscopy (IR) analyses absorption and transmission of infrared light. Absorbed energy of certain wavelengths of light is transformed into vibrational and/or rotational energy, based on the selection rules from quantum chemistry, and this results in lack of transmitted photons falling onto a detector. This creates fingerprints in spectrum that are unique for each molecular structure. Fourier transform IR was developed for faster measurements as it allows IR to scan all frequencies simultaneously. However, simultaneous measurements resulted in

a spectrum that showed intensity for every frequency, so mathematical technique called Fourier transformation is necessary to process each individual frequency and provide spectrum that is possible to interpret.

FT-IR is suitable for differentiation of various types of acid sites, their concentration, and their localisation on their surface or inside of their pores. Acid sites present in zeolites are characterised by analysing infrared spectrum of probe molecules which are adsorbed on those sites. Most used probe molecule is pyridine, because of its distinctness from pyridinium ions, that makes differentiation between acid site types possible. The absorption lines of pyridinium ion tend to be around 1540 cm^{-1}, indicating proton, or so called Brønsted acidity, while coordinatively bonded pyridine bands, indicating aprotic, therefore Lewis, acidity were found to be in region from 1440 cm^{-1} to 1465 cm^{-1}. [38] When necessary, other probe molecules, including deuterated acetonitrile, are used for studying acidity of zeolites. This is the case for studying zeolites with LTA framework, which have small pore openings.

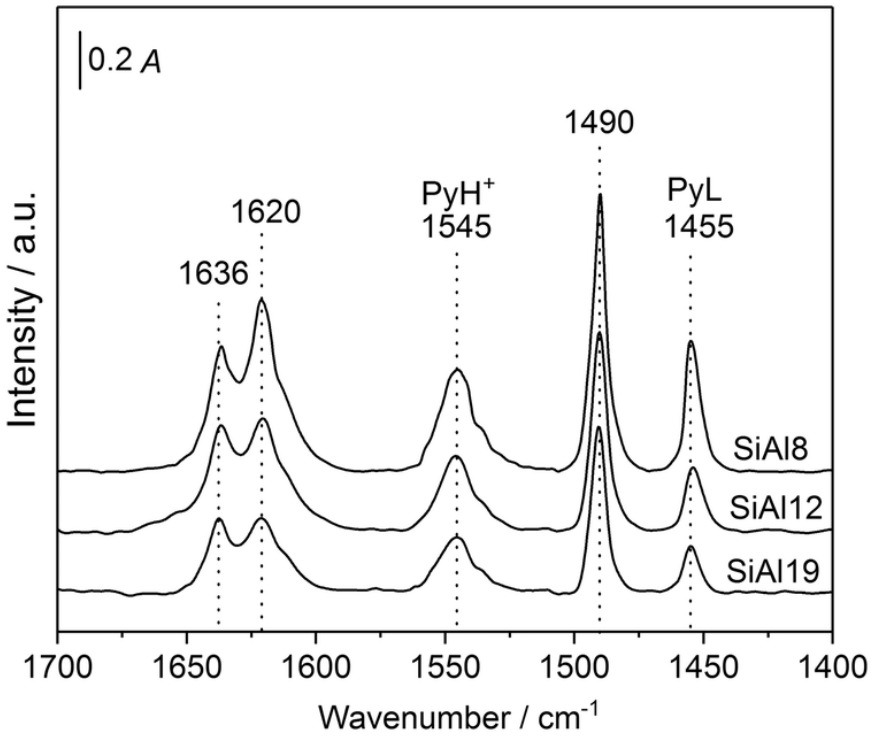

Figure 6: FTIR of pyridine adsorbed on BEA zeolite[39]

1.2.6. Inductively coupled plasma mass spectrometry

Inductively coupled plasma mass spectrometry (ICP-MS) is a technique used for very sensitive multi elemental analysis, as it has very low detection limits. Instrumentation of ICP-MS consists of several components including sample introduction system, which consists of nebulizer and spray chamber, creating fine aerosol and filtering the droplets based

on their size. Inductively coupled plasma is used for ionisation of the sample. Ion optics are a set of electrostatic lenses used for guiding the ionised sample towards mass analyser. Passing ions are filtered by their mass to charge ratio by quadrupole, which is one of the commonly used mass analysers. Ions then hit the detectors, which are most often electron multipliers, and result in signals that can be then quantified. Quantification of the signals is most often done by comparison with standards of exactly known composition. [40]

2 Experimental part

2.1. UZM-9 synthesis

Zeolite UZM-9 was synthesized by hydrothermal synthesis following reference[18]. Procedure involved dissolving aluminium hydroxide in the mixture containing 19.96 g of TEAOH (35% aqueous solution) and 16.35 g of diethyldimethylammonium hydroxide (DEDMAOH, 20% aqueous solution), while being stirred mechanically at 175 rpm. 11.07 g of silica (Ultrasil VN-3) was added into the mixture, resulting in dense white gel. Second mixture consisting of 0.45 g of sodium hydroxide dissolved in 4.18 g of tetramethylammonium (TMAOH, 25% aqueous solution) and 9.79 g of water was then added into the beaker with the stirred mixture. The resultant mixture was then homogenized for 30 minutes. The molar composition of mixture was 1.0 SiO_2 : 0.16 $Al(OH)_3$: 0.22 TEAOH : 0.15 DEDMAOH : 0.06 TMAOH : 0.06 NaOH : 11.16 H_2O. (Synthesis 1)

Following the homogenization, the mixture was transferred into 90 mL teflon lined stainless steel autoclaves. Autoclaves were heated at 150 °C both under agitation and static conditions for 5 and 6 days, respectively. Samples were collected after 1, 2, 4, and 5 days (agitation), and after 2, 5, and 6 days (static conditions). Extensive sampling resulted in lack of product for further samples and the synthesis was therefore stopped. The autoclaves were first cooled down by stream of water and then put back into the oven after the samples were collected. Solid content was washed with distilled water, centrifuged at 3000 rpm for 5 minutes and dried in the oven at 60 °C overnight.

Additional syntheses were performed by following the same procedure as described previously, only some synthesis parameters such as temperature, SDA, addition of crystal seeds, and the sources of silica (Ultrasil VN-3 for syntheses 1-9 and Cab-O-Sil M5 for every following synthesis) were changed. Synthesis mixtures were prepared in various amounts, based on the sizes of autoclaves, but their molar compositions stayed the same. Table 1 shows every synthesis, its difference from the one described above, either by temperature, agitation, seeding, the amount of SDAs, and the effects of those changes on crystallization length and their Si/Al ratios. Some of the syntheses in Table 1 are shown without the time of full crystallinity, as a result of insufficient amount of produced material for further characterization due to extensive sampling or far too long crystallization times making them undesirable.

Table 1: List of syntheses

Synthesis	T [°C]	Agitation	Seeding	SDA	observed crystallinity [days]	fully crystalline [days]	Si/Al in mixture	Si/Al ICP-MS
patent[18]	150	-	-	100%	-	3	-	5.2
1	150	yes	-	100%	2	-	6.35	-
2	150	no	-	100%	6	-	6.35	-
3	125	yes	-	100%	-	-	6.35	-
4	125	no	-	100%	-	-	6.35	-
5	150	yes	-	100%	4	-	6.35	-
6	150	no	-	100%	5	-	6.35	4.2
7	150	yes	1%	100%	2	2	6.35	3.6
8	150	yes	1%	100%	1	1	6.34	-
9	150	yes	0.5%	100%	1	1	6.28	-
10	150	yes	1%	70%	1	-	6.35	-
11	150	yes	0.5%	70%	1	-	6.35	-
12	150	yes	1%	100%	0.25	1	6.35	-
13	150	yes	0.25%	100%	1	1	6.35	-

Successfully synthesised zeolites, with diffractograms corresponding to literature were chosen for characterisation and calcined. Calcination took 6 hours at 520 °C (temperature ramp. 1°C/min.) under nitrogen gas flow for the first two hours and then under air flow for the remaining 4 hours.

2.2. Ion exchange

Calcined zeolites containing sodium cations were ion exchanged for ammonium, lithium, and potassium cations using 100mL/g of 1M solutions of ammonium nitrate (NH_4NO_3), lithium chloride (LiCl), and potassium nitrate (KNO_3). Zeolite samples were stirred at room temperature for 3 hours, after that centrifuged and decanted. This process was repeated three times, always using new batch of solutions. After the last exchange, the samples were washed with water, centrifuged, decanted, and left to dry.

2.3. Direct synthesis of Fe and Zr form of UZM-9 zeolite

The synthesis of Fe- and Zr- form of UZM-9 zeolite was done by the full replacement of Al, following the previous procedure.[18] Iron(III) nitrate nonahydrate ($Fe(NO_3)_3 \cdot 9H_2O$) and zirconium isopropoxide isopropanol complex ($Zr(OCH(CH_3)_2)_4 \cdot (CH_3)_2CHOH$) were used as sources of chosen elements.

The mixture containing 36.23 g of TEAOH (35% aqueous solution) and 34.94 g of DEDMAOH (20% aqueous solution) was mixed with 25.03 g of $Fe(NO_3)_3 \cdot 9H_2O$ under mechanical stirring. Addition of silica (Cab-o-Sil M5), with calculated amount being 23.45 g, was done gradually for better homogenization and dissolution. Mixture became too dense and dry for stirring, most probably due to used silica source and a lack of water, or rather Fe source being in form of nonahydrate with large amount of water being bound in the molecules, instead of added into mixture later. A solution containing 0.97 g of NaOH dissolved in 8.92 g of TMAOH (25% aqueous solution) and 11.27 g of distilled water was added into previous mixture, in order to dissolve more of the silica. As a result, more, but not all aforementioned amount of silica was added, with final amount being 21.25 g. This mixture was left to stir for another 30 minutes, which yielded no apparent gains on the density or homogeneity of mixture, so it was further homogenised by hand, using spatula. Resulting mixture was divided into halves and one was mixed with 0.70 g of seeding crystals from previous synthesis. Mixtures were put into teflon lined stainless steel autoclaves, put into an oven, and heated at 150 °C under agitation. Composition of synthesis mixture, with the lowered amount of SiO_2, was 1.0 SiO_2 : 0.18 $Fe(NO_3)_3$: 0.24 TEAOH : 0.17 DEDMAOH : 0.07 TMAOH : 0.06 NaOH : 12.48 H_2O.

Zirconium form of UZM-9 zeolite was prepared by dissolving 22.49 g of $Zr(OCH(CH_3)_2)_4 \cdot (CH_3)_2CHOH$ in solution containing 33.92 g of TEAOH (35% aqueous solution) and 32.71 g of DEDMAOH (20% aqueous solution). 22.13 g of silica (Cab-o-Sil M5) were then gradually added into mixture that was mechanically stirred until fully dissolved, which resulted in paste-like mixture. Lastly, a solution of 0.91 g of NaOH dissolved in 19.96 g of distilled water and 8.35 g of TMAOH (25% aqueous solution). Prepared mixture was then homogenized for 30 minutes under mechanical stirrer and then divided into two parts. One part was mixed with 0.70 g of seeds from previous synthesis. Mixtures were then poured into teflon lined stainless steel autoclaves and heated at 150 °C under agitation. Their composition was 1.0 SiO_2 : 0.16 $Zr(OCH(CH_3)_2)_4 \cdot (CH_3)_2CHOH$: 0.22 TEAOH : 0.15 DEDMAOH : 0.06 TMAOH : 0.06 NaOH : 11.22 H_2O.

2.4. Experimental charge density matching approach

Synthesis followed article[41], with changes in used reagents, using TMAOH instead of TMACl. Composition of synthesis mixture was 1.00 SiO_2 : 0.40 TEAOH : 0.05 TMAOH : 0.03 $(Al[OCH(CH_3)C_2H_5]_3$: 0.02 M, where M is LiCl or NaCl. The mixture, without the source of M, was divided into three beakers – containing Na^+ (i) and Li^+ (ii) ions, and one free of Na^+

and Li^+ (iii) ions. Prepared mixtures were left to stir for one day at room temperature and afterwards transferred into teflon inserts which were then put into stainless steel autoclaves. Autoclaves were put into an oven at 100 °C and synthesis continued for 13 days. Samples were collected after 10 and 12 days. Solid material from autoclaves was centrifuged, decanted, and washed with distilled water. Finally, it was left to dry in an oven at 60 °C and then characterised by XRPD.

2.5. Instrumentation

Diffractograms of prepared samples were collected on a Bruker D8 Advance diffractometer equipped with energy dispersive detector LYNXEYE XE-T using Cu Kα radiation. Measurements were carried out in range from 3 to 40°. Samples were prepared by grinding larger pieces of prepared and dried product into fine powder, which was then transferred into plastic holders, which were put into the instrument.

Porosity and texture properties of samples were evaluated by measurements on Micrometrics 3Flex volumetric Surface Area Analyzer using Nitrogen adsorption and desorption isotherms at -196 °C. At first, the turbomolecular pump vacuum (Micromeritics Smart Vac Prep instrument) was used to outgas samples at 110 °C for one hour, until the pressure of 13.3 Pa was reached, starting from ambient temperature with a heating rate of 1 °C/min. After that, the temperature was increased to 250 °C with the same heating rate and kept to heat for 8 hours. Brunauer-Emmet-Teller method (BET) was used for calculation of specific surface area using adsorption data in range of relative pressures $p/p = 0.05\text{-}0.20$.[34, 42, 43] Micropore volume and external surface area were evaluated by the t-plot method. [42 44] Total adsorption capacity was determined by adsorbed amount at relative pressure of $p/p_0 = 0.95$.[42]

^{27}Al MAS NMR and ^{29}Si CPMAS NMR experiments were carried out on JEOL JNM-ECZR 600 MHz, with shielded magnetic field of 14T, with the frequency of rotor, used for MAS, being 18 kHz and its diameter 3.2 mm.[45] The rotor was uniformly packed with zeolite sample and placed into the probe, which was then inserted into the spectrometer. The spinning of rotor was increased gradually until reaching the desired values, while monitoring the drive and bearing pressure, to mitigate any potential damage. The probe was manually tuned and matched, to reach optimal values for reflection dip and value. Saturation recovery experiments were conducted to determine the relaxation times of the measured samples, which are necessary for setting up the measurement. The ^{27}Al MAS NMR measurement was conducted using a soft excitation pulse, allowing the use of fictitious ½ spin instead of quadrupolar one, that belongs

to ^{27}Al nucleus. The ^{29}Si spectrum was measured by CPMAS experiment, transferring coherence from nearby ^{1}H nuclei.

Concentration of Brønsted and Lewis acid sites as well as framework Si/Al ratio was determined by adsorption of d_3-acetonitrile and consequent FTIR spectroscopic measurement. Nicolet 6700 equipped with AEM module and a resolution of 4 cm^{-1} was used to measure the FTIR spectra. Prepared samples of zeolites were first pressed into wafers, which had density in range of 8.0 – 12 mg/cm^2 and then activated by outgassing at 450 °C into the IR cell, while being under the vacuum. Acetonitrile was degassed before adsorption, which was carried out at room temperature, took 20 minutes, and the partial pressure was 5 Torrs. Desorption took 20 minutes. The spectra were then recalculated on wafer density of 10 mg/cm^2. Evaluation of concentration and type of acid sites used the molar absorption coefficients for d_3-acetonitrile adsorbed on Brønsted acid sites ((C≡N)-B at 2297 cm^{-1}, $\varepsilon_B = 2.05 \pm 0.1$ $cm \cdot \mu mol^{-1}$) and strong and weak Lewis acid sites ((C≡N)-L_1 at 2325 cm^{-1}, (CN)-L_2 at 2310 cm^{-1}, $\varepsilon_L = 3.6 \pm 0.2$ $cm \cdot \mu mol^{-1}$) .[46, 51]

ICP-MS was used to determine chemical composition of samples, using Agilent 7900 ICP-MS. Process of sample preparation consisted of mixing approximately 50 mg of the sample with 1.8 mL of HNO_3 (67-69%, ANALPURE®), 5.4 mL of HCl (34-37%, ANALPURE®), and 1.8 mL of HF (47-51%, ANALPURE®) in a Teflon vessel, which was left open for 20 minutes and then closed and placed into microwave (Speedwave® XPERT, Berghof) for 25 minutes, while being heated at 250 °C with heating rate of 5 °C/min. Mixture was then left to cool down and surplus of HF was captured into complex by addition of 12 mL of concentrated H_3BO_3 solution and then heated in the microwave at 190 °C (5 °C/min) for 10 minutes. The obtained solution was left to cool down and then diluted by distilled water to 50 mL for analysis.

3 Results and discussion

3.1. Synthesis of UZM-9 zeolite

The crystallinity and phase purity of prepared zeolites were characterised by XRPD and their diffractograms correspond to those in IZA[19] and literature[18]. The procedure from patent was successfully reproduced[18], with crystalline product starting to form already after fourth day of synthesis under agitation (Synthesis 5) and sixth day while being static (Synthesis 6). It was shown that decreasing synthesis temperature from 150 °C to 125 °C does not lead to desired products even after 8 days and that is why it was stopped and not prolonged anymore (Syntheses 3 and 4). Based on XRD patterns, only sample from Synthesis 5, from Table 1, was further characterised.

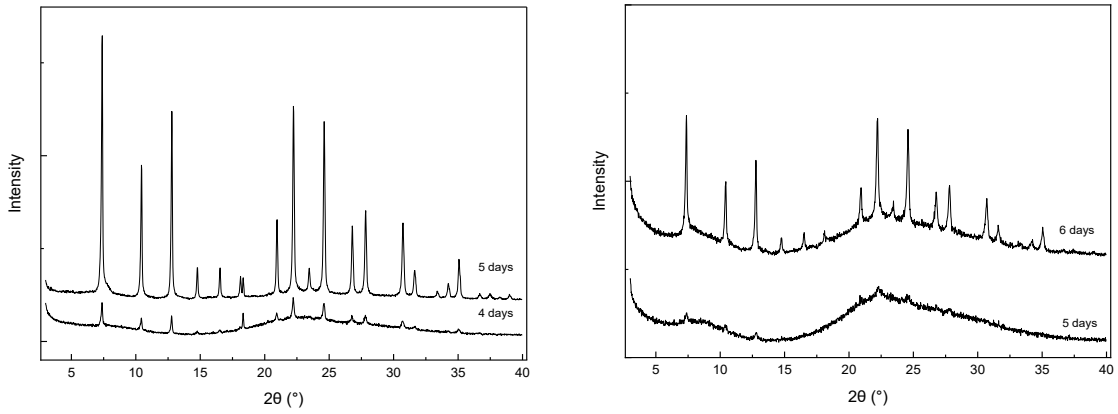

Figure 7: Diffractograms of UZM-9 zeolite from agitated (Synthesis 5, left) and static synthesis without seeding (Synthesis 6, right)

Diffraction lines in the case of agitation (Figure 7, left) show signs of appearing diffractions, and therefore presence of crystalline product, after 4 days. Although, some amorphous phase is present, which is clear from overall lack of flat baseline and particularly high background at angles between 20-25°. The diffraction line after 5 days of synthesis shows significant increase in crystallinity as there are peaks with high intensities and almost flat baseline. Static synthesis (Figure 7, right) shows formation of crystals after 6 days of synthesis. There is still abundance of amorphous phase present in product, but there is clear distinction between the diffraction line from sixth and the one from the fifth day, which shows almost fully amorphous material. Both syntheses were stopped due to lack of material for sampling.

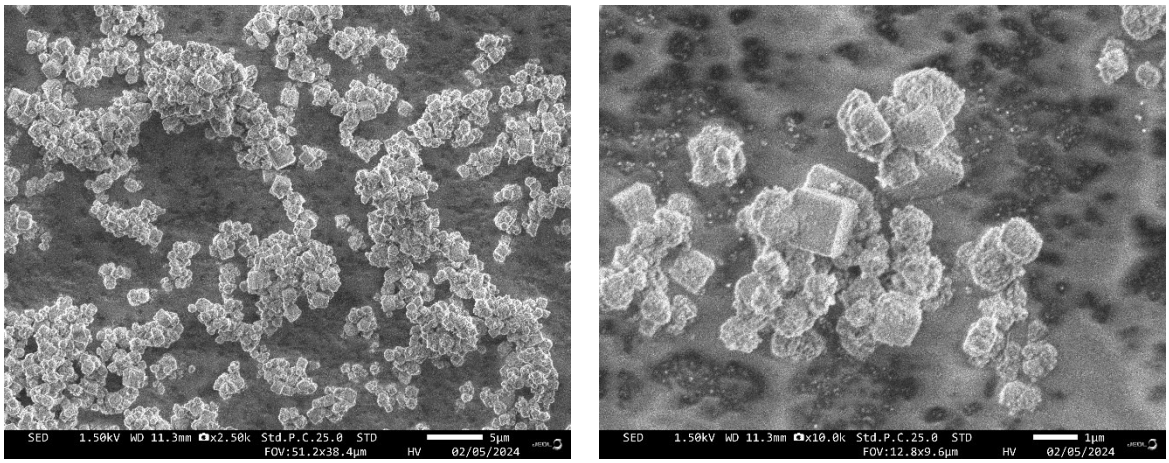

Figure 8: SEM image of UZM-9 zeolite from agitated synthesis without seeding (Synthesis 5)

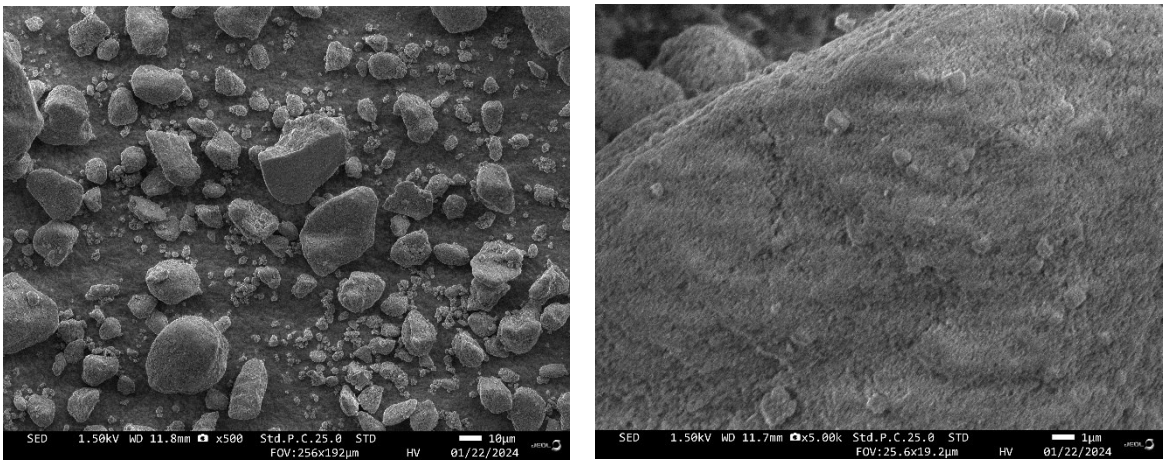

Figure 9: SEM image of UZM-9 zeolite from static synthesis after 5 days (Synthesis 6)

SEM images in Figure 8 show crystals, which have cubic shape with varying sizes around 1 µm. Some have their edges and faces well-defined while others show presence of another unknown phase, with rough texture, on their surface, possibly corresponding to the high background of XRD diffractograms. This creates irregularities and roughness in the shapes of crystals. Coverage of the zeolite crystals by the unknown material is not uniform and ranges from larger deposits to almost clean surfaces. Unknown phase may be composed of yet uncrystallized precursor, which means that synthesis should have been prolonged, but it is also possible that it is some other material, with possibilities being some form of SiO_2, Al_2O_3, or another type of zeolite. The SEM images in Figure 9 show solid material with presence of small cubes. Comparing it to XRPD diffraction lines from Synthesis 6 in Figure 7 on the right, could explain the mostly amorphous phase, with small signs of crystallinity rising from the presence of the small cubes, which could already be forming UZM-9 zeolites.

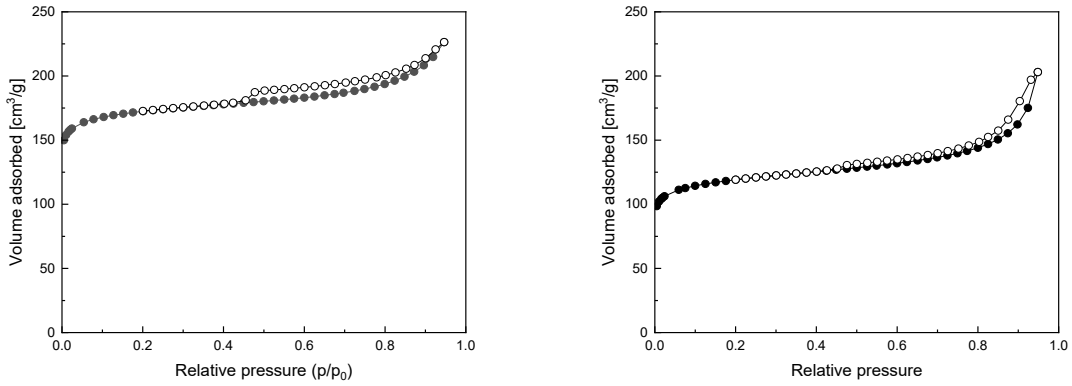

Figure 10: Adsorption/desorption isotherms of UZM-9 zeolite from agitated (Synthesis 5, left) and static synthesis without seeding (Synthesis 6, right)

Nitrogen adsorption isotherms, shown in Figure 10, were used to calculate texture properties of prepared UZM-9 zeolite. Their shape may be classified as Type I(a) isotherm, characteristic of microporous materials, with primarily narrow micropores.[33] Material prepared by static synthesis shows much worse properties than the ones prepared under agitation, with largest difference in BET surface area as shown in **Chyba! Nenašiel sa žiaden zdroj odkazov.**. While the BET, micropore and total pore volumes show larger values for agitated synthesis, the external surface area goes against this trend, with values similar for both syntheses, considering the measurement error. Presence of amorphous phase, in the static synthesis, is most probably the reason for observed differences, although it is probable that it was also affected by agitation. Crystals, their size, or the size of their aggregates may have been affected by agitation, resulting in differences that could have affected the surface properties. The values from reference[18] correspond to those from agitated synthesis (Synthesis 5).

Table 2:Porosity and surface properties of UZM-9 zeolite measured by nitrogen adsorption/desorption isotherms

Synthesis	BET [m^2/g]	$S_{external}$ [m^2/g]	$V_{micropore}$[cm^3/g]	V_{total}[cm^3/g]
static	427	97	0.14	0.31
agitated	605	91	0.23	0.35

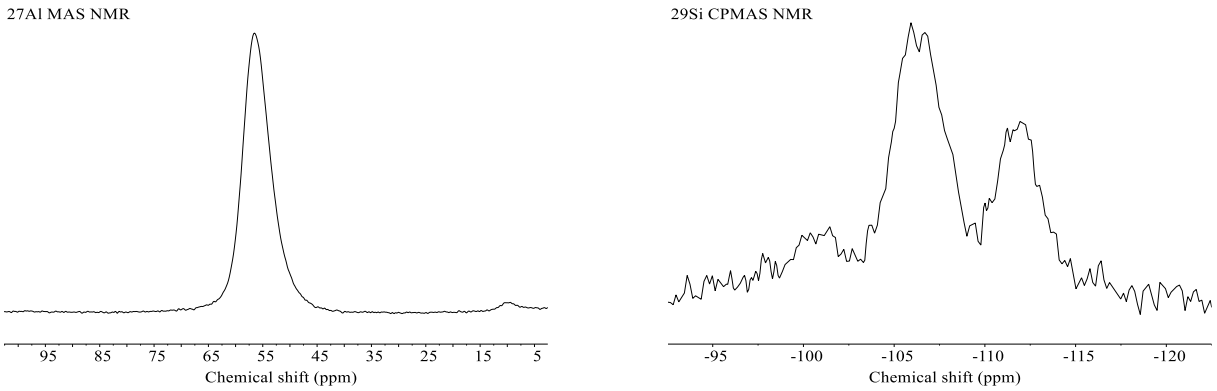

Figure 11: ^{27}Al MAS NMR and ^{29}Si CPMAS NMR spectra of UZM-9 zeolite from synthesis without seeding

In the ^{27}Al MAS NMR spectrum, notable peaks appear at around 55 ppm, which corresponds to tetrahedrally coordinated aluminium, with fairly symmetric peak suggesting regular environment of aluminium atoms without many distortions or various aluminium sites. The ^{29}Si CPMAS NMR spectrum shows peaks in the range of -95 to -115 ppm, which correspond to the Si atoms having various amounts of AlO_4 tetrahedra in its surroundings. The peaks correspond to Si atoms being connected to two, three or four AlO_4 tetrahedra at around -103, 107, and 112 ppm respectively, as shown in reference[47]. Those are consistent with literature and confirm the tetrahedral structure of prepared material.[19, 36]

ICP-MS was used for determination of elemental composition of the zeolites from agitated synthesis. Si/Al ratio of prepared zeolite was 4.2, which is lower than zeolite prepared in patent[18] with Si/Al = 5.2.

3.2. Effect of seeding and amount of SDA

Seeding is well known to promote crystallization of desired structure, shorten synthesis time and also the ability to reduce or eliminate the need for organic SDAs. Seeding the aforementioned synthesis at the level of 1% resulted in fully crystalline material already after two days of agitated synthesis, as was visible by flat baseline and the presence of characteristic diffraction lines, compared to diffractogram from patent, confirmed synthesis of UZM-9 zeolite. Samples from syntheses 7, 10-14 were further characterised.

Results of Syntheses 10 and 11 with the amount of SDAs decreased to 70 %, showed presence of amorphous phases even after 5 days of synthesis, thus making them unviable.

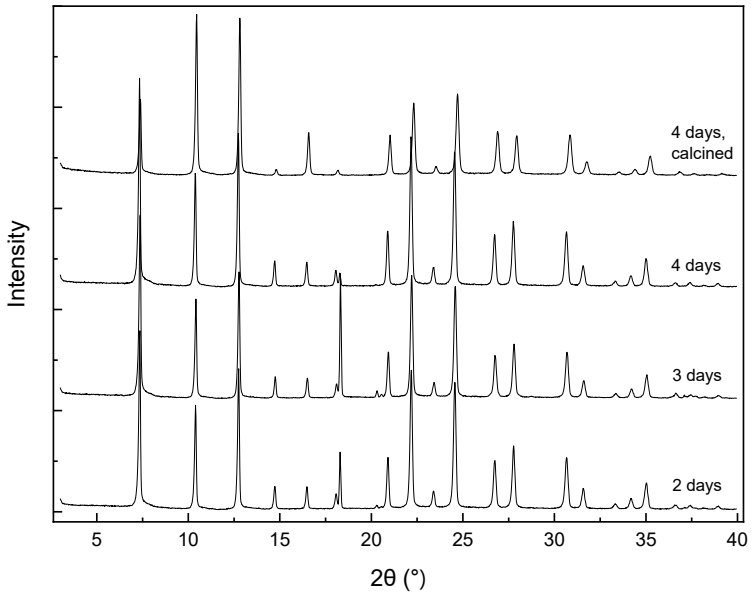

Figure 12: Diffractograms of UZM-9 zeolite synthesised with seeding showing differences changes after 2, 3, 4 days of synthesis and calcined product (Synthesis 7)

Diffraction lines show that even though product is fully crystalline after two days, there are changes in the intensities of double peak occurring around 18°, until its change into single peak after calcination, while the peak at around 17° increases. At that point, the diffractogram completely corresponds to one from patent. This may be a result of structural change while being calcined when SDAs and organic residues are removed at elevated temperature. Seeded synthesis (Synthesis 7), with its completely flat baseline, indicates that previous synthesis was not fully completed, resulting in its high background.

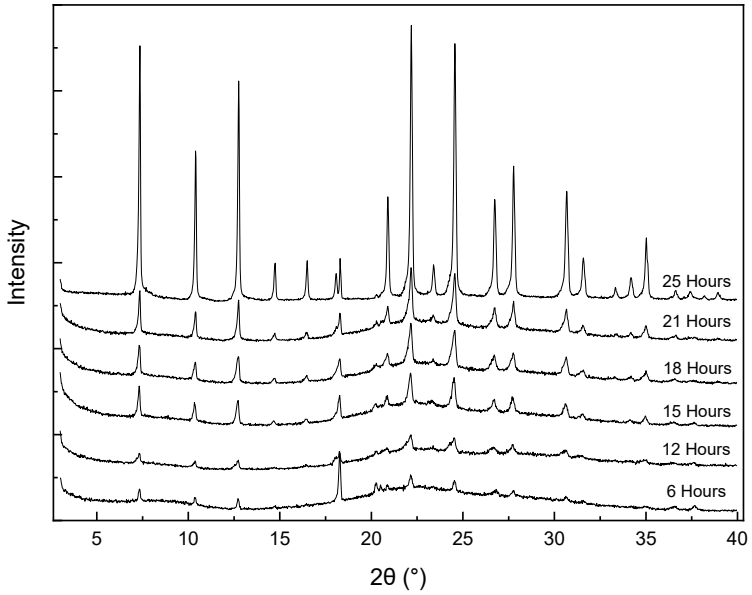

Figure 13: Kinetics of UZM-9 synthesis with seeding (Synthesis 12)

Crystallization kinetics of UZM-9 synthesis (Synthesis 12) were studied by addition of seeds from material prepared in Synthesis 7, starting from 6 hours and periodically collecting samples until the end of synthesis after 25 hours. The first sign of crystallization was observed already after 6 hours, with gradual increase in intensities of corresponding diffraction lines, until becoming fully crystalline at some point between 21 and 25 hours. No further samples were taken due to the lack of prepared material. Results are shown in Figure 13, which confirms presence of UZM-9 zeolite, as it corresponds to literature.[18,19] Another thing to note is formation of double peak at around 17° between 21 and 25 hours of synthesis time, which is also visible in Figure 12, only disappearing after calcination as discussed above, possibly being a result of SDA presence.

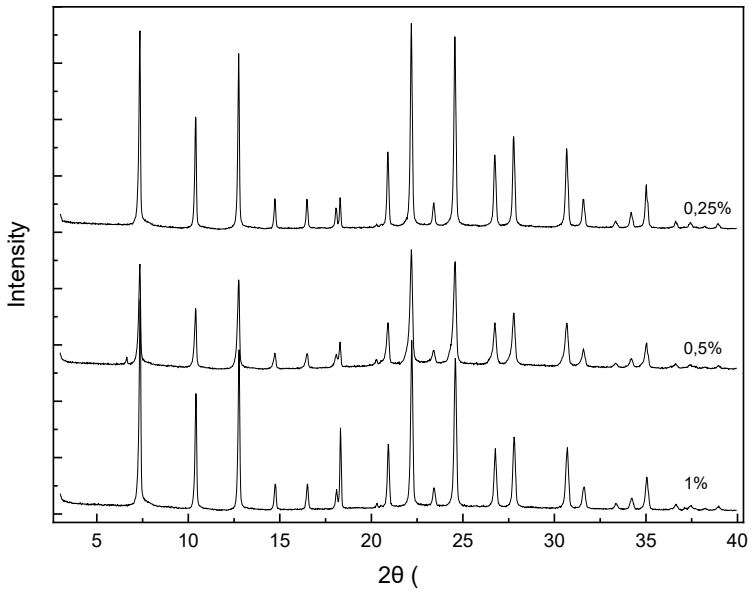

Figure 14: Diffractograms of UZM-9 zeolite from syntheses with different amounts of seeding crystals after 24 hours of synthesis (Synthesis 9, 12, 13)

Lowering amounts of seeding crystals from 1 % to 0.25 % is shown in Figure 14, which shows diffractograms of material collected after 24 hours of synthesis (Syntheses 9, 12, and 13). Lowering amount of seeding crystals up to 0.25 % does not seem to affect duration of synthesis, suggesting possibility of its further decrease.

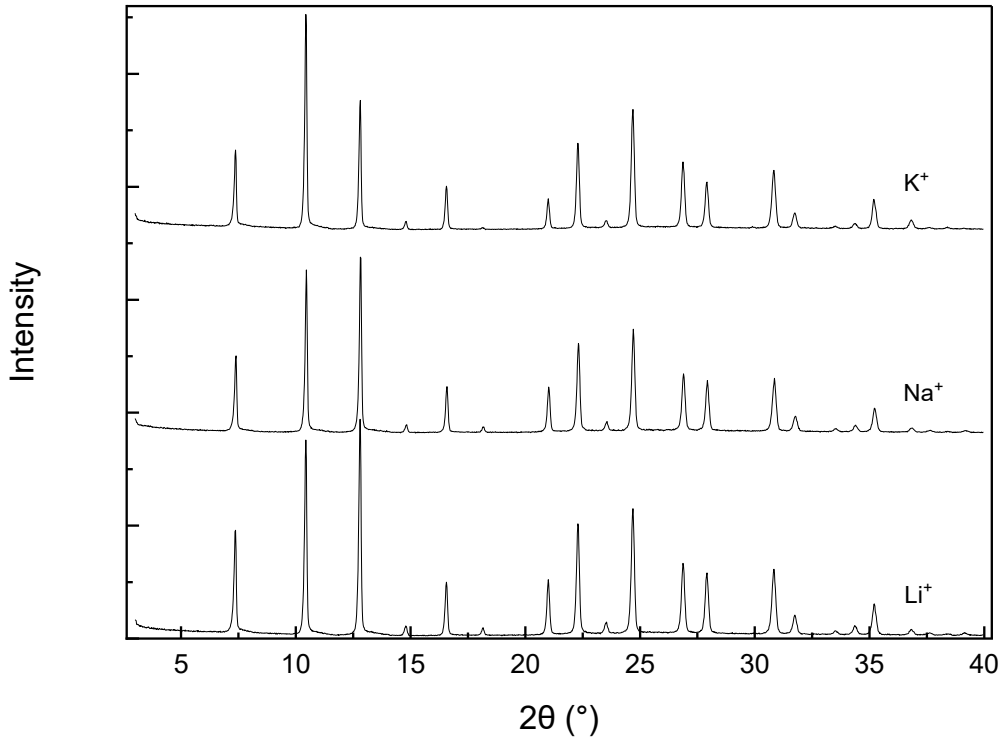

Figure 15: Diffractograms of ion exchanged UZM-9 zeolite (Synthesis 7)

Diffractogram in Figure 15, with diffraction lines of ion exchanged forms of UZM-9 zeolite, show only slight difference in intensities of peaks from the as-synthesised Na-UZM-9, therefore denying possibility of ion exchange severely changing the structure of prepared material. The differences in intensities of diffraction lines in Figure 15, as opposed to Figure 14 are a result of calcination.

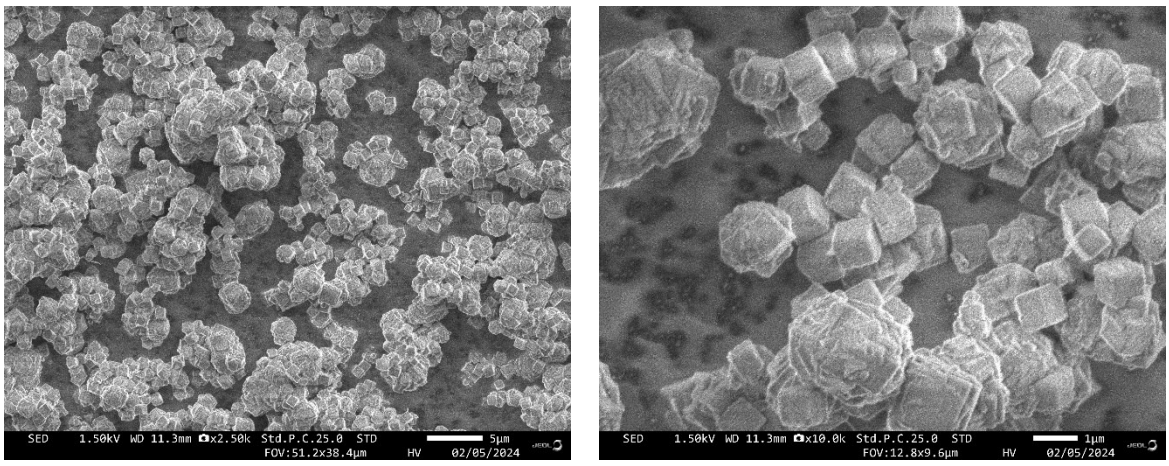

Figure 16: SEM images of UZM-9 zeolite from seeded synthesis with different scales, 5 µm on the left and 1 µm on the right (Synthesis 7)

Crystals from seeded synthesis in Figure 15 show sizes ranging around 1 μm, which is the same as synthesis without seeding, but they are much more defined, with much less of the unknown phase discussed previously. This may explain the difference between porosity of materials synthesised with and without seeding due to the amorphous phase possibly blocking the pores. Another possibility may be overall lower amount of porous material in sampled material, therefore having lower amount of adsorbed molecules. The presence of structures with many edges and what seems to be corners of intertwined cubes, is another difference between seeded synthesis shown in SEM images in Figure 16 and synthesis without seeding shown in Figure 8.

As synthesised, and ion exchanged zeolites (Synthesis 7) were characterised by gas adsorption, namely nitrogen (N_2) and carbon dioxide (CO_2), to study their effects on the porosity and surface properties.

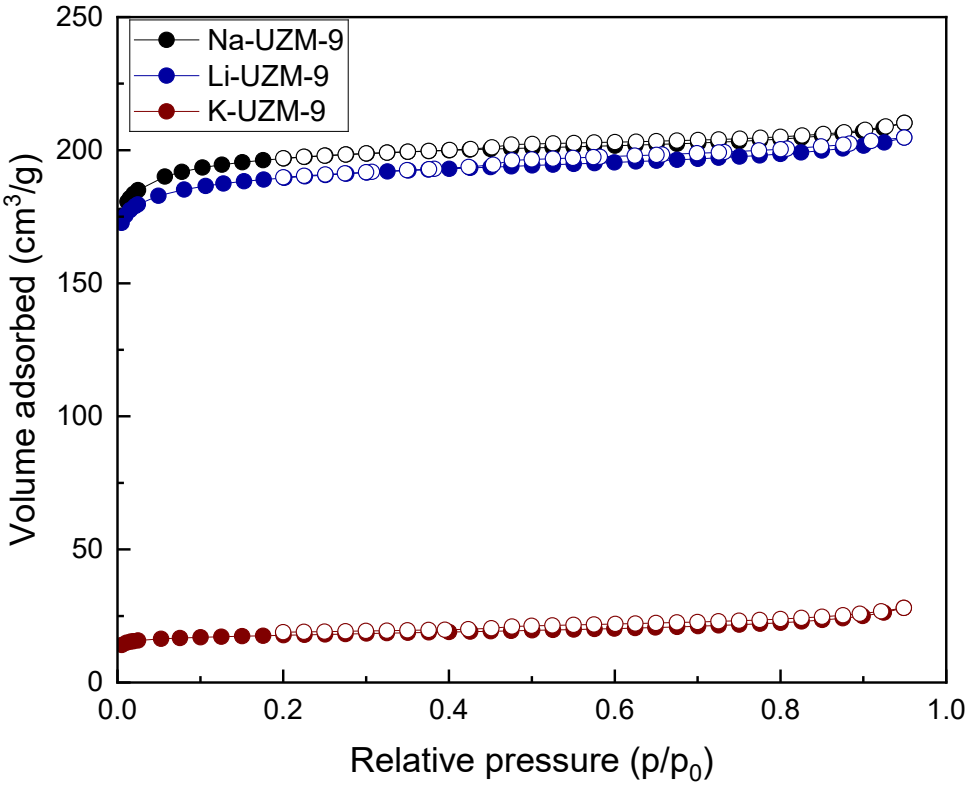

Figure 17: Nitrogen adsorption/desorption isotherm of UZM-9 zeolite from synthesis with seeding (Synthesis 7)

N_2 adsorption/desorption isotherm was used to study Na^+, Li^+ and K^+ ion-exchanged forms of UZM-9 zeolite and the results are shown in Table 3. Samples from seeded synthesis

(Synthesis 7) have larger BET surface areas and micropore volumes than the ones from synthesis without seeding (Synthesis 5, **Chyba! Nenašiel sa žiaden zdroj odkazov.**), while having lower values in total pore volumes and external surface areas as shown in Table 3. Cations present in UZM-9 zeolite affect its porosity and surface properties, as the values of BET surface areas, micropore and total pore volume stay similar for Li-UZM-9 and Na-UZM-9, while K-UZM-9 zeolite shows much lower values. This is probably a result of 8 ring openings of the UZM-9 framework, where the presence of large cations blocks the entrance for nitrogen molecules, which have kinetic diameter of 364 pm.[48]

Table 3: Porosity and surface properties of UZM-9 zeolite measured by nitrogen adsorption/ desorption isotherms in its various ion exchanged forms (Synthesis 7)

Zeolite form	BET [m^2/g]	$S_{external}$ [m^2/g]	$V_{micropore}$[cm^3/g]	V_{total}[cm^3/g]
Li-UZM-9	640	68	0.26	0.32
Na-UZM-9	646	73	0.27	0.32
K-UZM-9	73	41	0.02	0.08

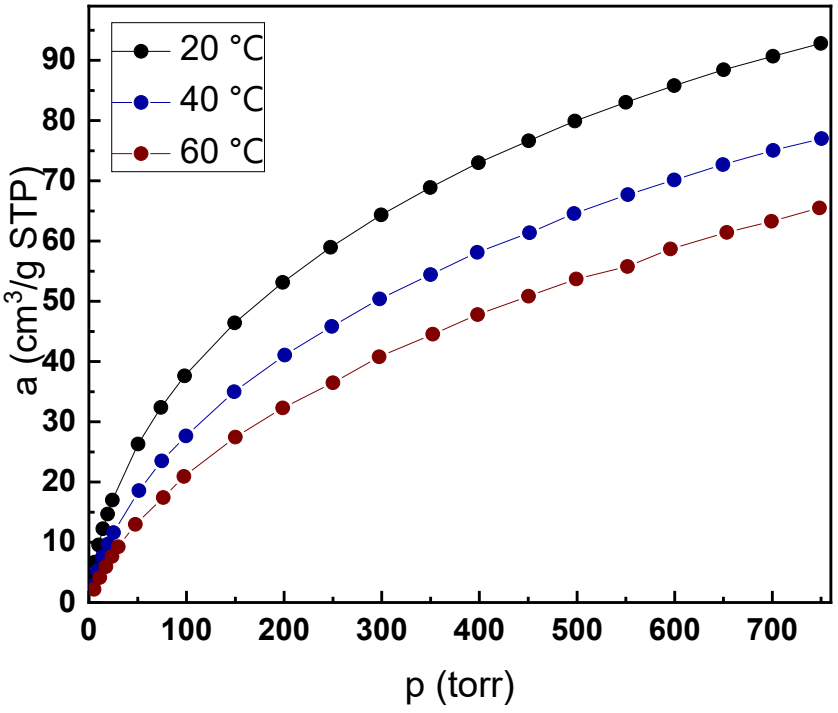

Figure 18: CO_2 adsorption isotherms of Na-UZM-9 zeolite at various temperatures (Synthesis 7)

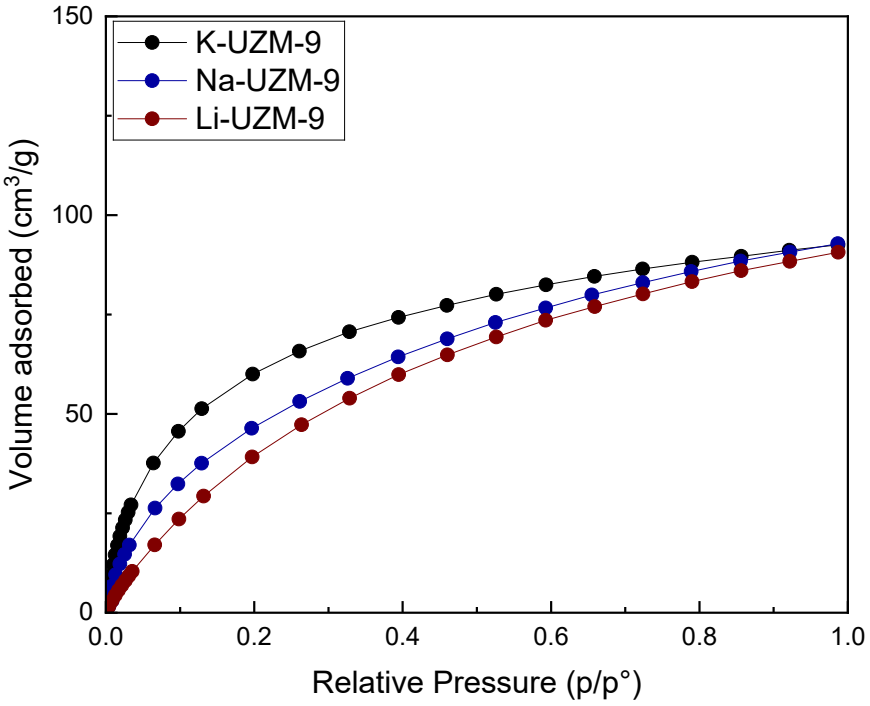

Figure 19: CO_2 adsorption isotherms of UZM-9 zeolite with exchanged ions measured at 20 °C (Synthesis7)

Adsorption isotherms in Figure 18 show dependence of CO_2 adsorption on temperature, with decrease of adsorbed amount at higher temperatures. Adsorption isotherms of CO_2 , in Figure 19, show dependence of adsorbed amount on ion exchanged form of UZM-9 zeolite The total adsorbed amount of CO_2 is practically the same, regardless of the cation, there are differences in uptake depending most probably on cation sizes, with the highest values when potassium cations are present and the lowest in presence of lithium cations, which suggests decreasing adsorption properties with decreasing cation size. It is possible that this is a result of CO_2 molecules interacting with the most accessible cations as well as the strength of interaction between CO_2 molecule and the cation.[49] Ion exchanged potassium cations present in UZM-9 do not seem to affect the adsorption of CO_2, which could be a result of smaller kinetic diameter of CO_2 (330 pm) as well as higher polarizability of CO_2 molecule leading to stronger interaction with potassium cations than N_2.[48]

Adsorption isosteres were created by plotting the logarithm of pressure (log p) to inverse value of temperature ($1/T$). Those values were taken from measured isotherms at constant temperature with corresponding pressure and set amount of adsorbed CO_2.[49] Isosteric adsorption heats were calculated from slopes of adsorption isosteres by equation

$$\mathrm{d}(\log p)/\mathrm{d}(1/T) = -\mathrm{q}_{st}/2.303 \cdot \mathrm{R}. \quad (4)$$

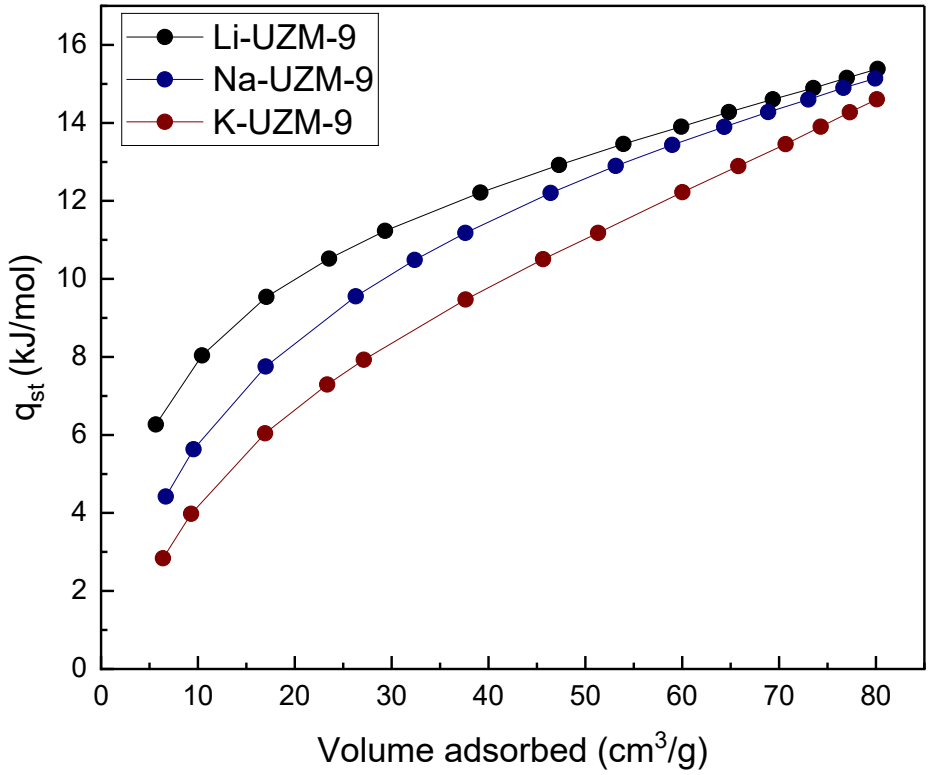

Figure 20: Isosteric adsorption heat dependence on adsorbed volume of CO_2 measured at 20 °C(Synthesis 7)

Figure 20 illustrates the relationship between isosteric adsorption heat and the adsorbed volume of CO_2, highlighting a trend of decreasing isosteric adsorption heat with increasing cation sizes. For the ion-exchanged UZM-9 forms, the plot lines exhibit a steep rise at lower adsorbed volumes, transitioning to a nearly linear increase at volumes exceeding 40 cm^3/g. At higher adsorbed volumes, the values show a converging tendency among the different UZM-9 forms studied.

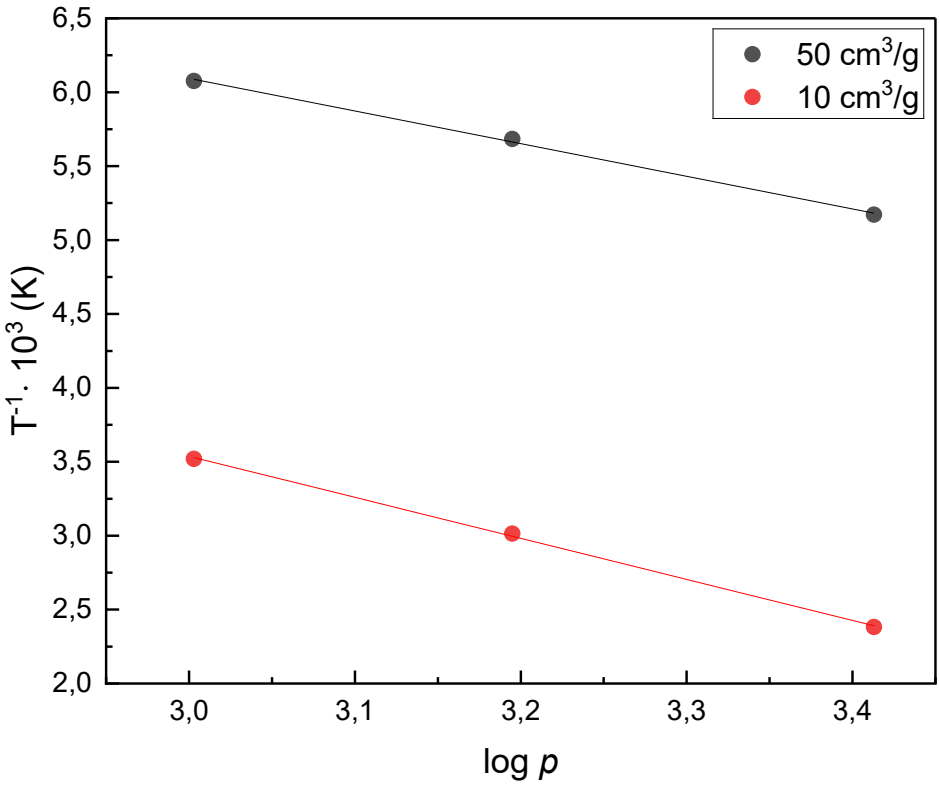

Figure 21: CO_2 adsorption isosteres of Na-UZM-9 zeolite (Synthesis 7)

Isosteres of Na-UZM-9, measured in range of 20-60 °C, are shown in Figure 21 and the isosteric adsorption heats of ion exchanged UZM-9 zeolites containing Li^+ , Na^+, and K^+ cations are shown in Table 4, at adsorbed amount of 50 cm^3/g and 10 cm^3/g. Values in Table 4 show highest values of isosteric adsorption heats from Li-UZM-9 at both adsorbed amounts. However, the amount decreases by larger margin at 10 cm^3/g of adsorbed amount. Decreasing cation sizes result in increasing isosteric adsorption heats with largest values belonging to Li^+ forms.

Table 4: Calculated isosteric adsorption heats at 20 °C for 50 cm^3/g and 10 cm^3/g of adsorbed CO_2

Zeolite form	$q_{st,50}$ [kJ/mol]	$q_{st,10}$ [kJ/mol]
Li-UZM-9	36	23
Na-UZM-9	34	18
K-UZM-9	31	14

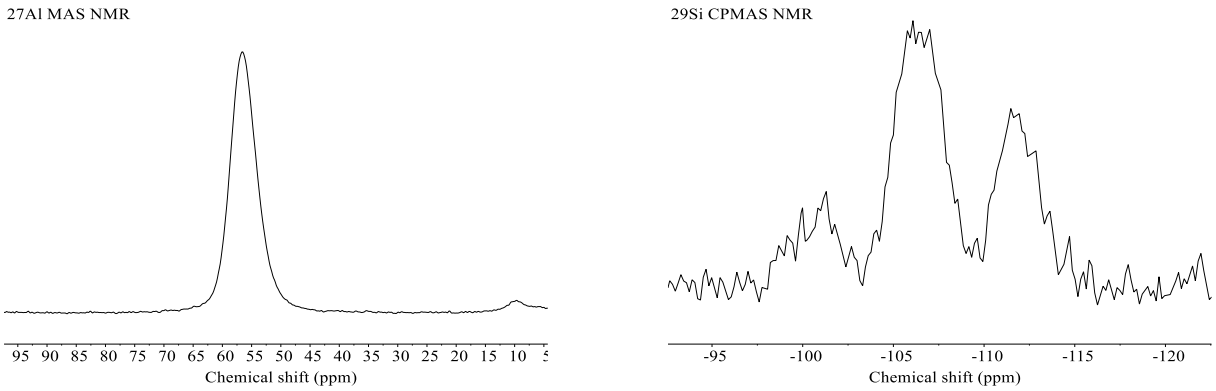

Figure 22: ^{27}Al MAS NMR and ^{29}Si CPMAS NMR spectra of UZM-9 zeolite from seeded synthesis (Synthesis 7)

The ^{27}Al MAS NMR and ^{29}Si CPMAS NMR spectra closely resemble those obtained from the synthesis without seeding, confirming the tetrahedral structure of the zeolite. Minor differences in intensities are observed in the Si spectrum, where the peak at -100 ppm remains consistent while the others diminish. The higher ratio of intensity for the peak at -100 ppm compared to the others suggests an even lower Si/Al ratio for the synthesis without seeding.[19,36]

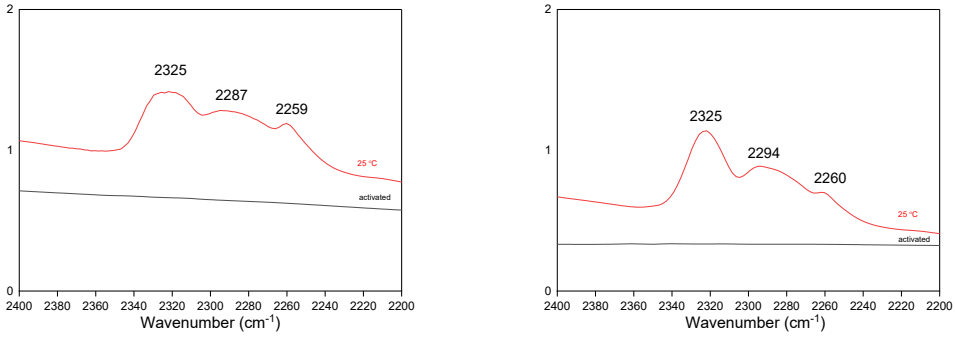

Figure 23: FTIR spectra of seeded synthesis (Synthesis 7, left) and synthesis without seeding (Synthesis 5, right)

The IR spectra were measured for synthesis without seeding (Synthesis 5) and with seeding (Synthesis 7) and are shown in Figure 23 The adsorption of d_3-acetonitrile resulted in appearance of bands at 2325 cm^{-1} , 2287 cm^{-1}, and 2259 cm^{-1} for seeded synthesis. For the synthesis without seeding the bands appeared at 2325 cm^{-1}, 2294 cm^{-1}, and 2260 cm^{-1}, which is a result of d_3-acetonitrile interacting with Brønsted and Lewis acid sites. The Si/Al ratio was also calculated from integrated intensities of peaks belonging to Brønsted and Lewis acid sites respectively by using molar extinction coefficients for d_3-acetonitrile. The results are shown in Table 5, with seeded synthesis showing that Si/Al ratios have higher values than the ones from ICP-MS chemical analysis, which means that there is more Si atoms in the framework of prepared material and therefore there are Al extra-framework Al species. Synthesis without seeding shows higher concentration of Brønsted acid sites. [47, 51]

Table 5: Results from FTIR analysis showing and Si/Al ratio of framework from synthesis with (Synthesis 7) and without seeding (Synthesis 5)

Seeding	C_B (mmol/g)	C_L (mmol/g)	Si/Al
No	0.52	0.02	4.11
Yes	0.32	0.02	3.83

The results of ICP-MS analysis have shown that zeolites prepared by seeded synthesis contain even higher amounts of aluminium within their framework. The Si/Al ratio is measured at 3.6 and 3.7 for the same synthesis mixture divided into two autoclaves, whereas it is 4.20 for synthesis without seeding. Table 6 presents the characterization results of ion-exchanged forms of UZM-9 zeolite, indicating a further decrease in the Si/Al ratio with decreasing cation sizes. Another thing to note is the Si/Na ratio, which shows, that as synthesised Na-UZM-9 zeolite contains much smaller amount of the cations in its pores, than the ion exchanged forms.

Table 6: Results of elemental analysis by ICP-MS of Li, Na and K forms of UZM-9 zeolite

	Si/Al	Si/Li	Si/Na	Si/K
Li-UZM-9	3.2	2.7	-	-
Na-UZM-9	3.3	-	75.4	-
K-UZM-9	3.4	-	-	3.9

3.3. Isomorphous substitution

The direct synthesis of Fe and Zr forms of UZM-9 was investigated following the procedure outlined in Example 6 of reference[18]. This involved an equimolar exchange of the Al for Fe or Zr, while also examining how the addition of UZM-9 seeds influences the product formation. However, compared to previous syntheses, difficulties were encountered early on in preparing the synthesis mixtures. They were too dry to homogenize properly, raising concerns about the even distribution of reactants and seeding crystals within the mixtures. This issue was particularly noticeable in mixtures containing iron, but those containing zirconium also proved to be a challenge to mix. As a result, the procedure had to be adjusted, specifically altering the order of chemical additions and also the source of silicon. All of the prepared mixtures were periodically sampled and characterised by XRPD, while observing the formation or changes in presence of peaks, suggesting crystallinity.

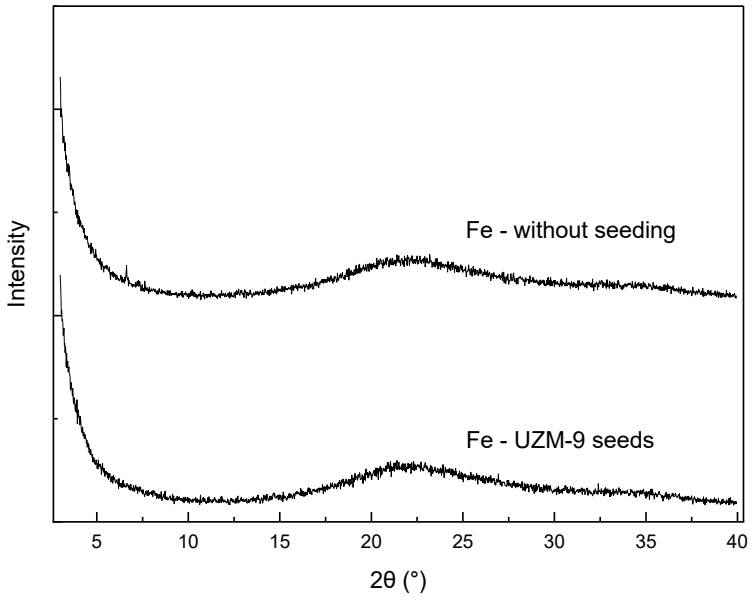

Figure 24 : Diffractograms of products after 19 days from synthesis with addition of Fe instead of Al atoms

The diffractograms in Figure 24 clearly demonstrate the absence of any crystalline product even after 19 days of synthesis. This led to the abandonment of the synthesis, as it was deemed either impossible to produce the desired materials or the synthesis duration was excessively long, making it undesirable.

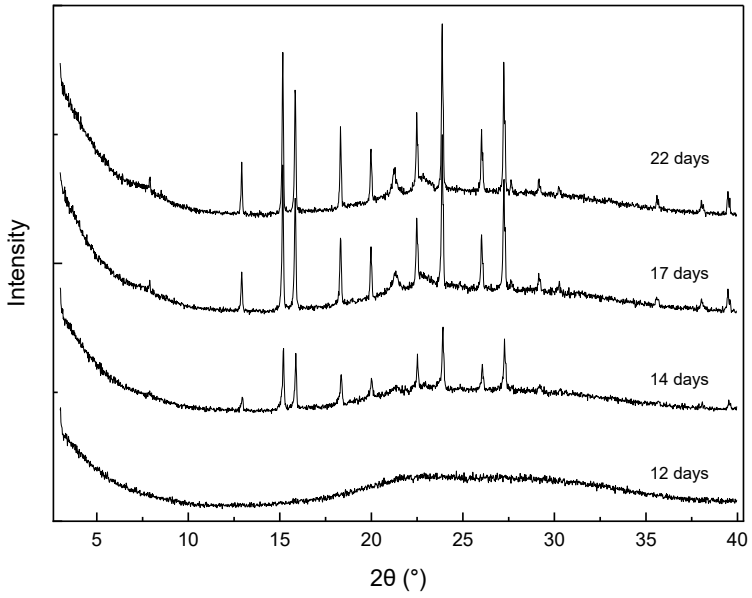

Figure 25: Diffractograms showing kinetics of crystallization from synthesis with isomorphous substitution of Al by Zr

Kinetics of crystallization of material prepared by synthesis with isomorphous substitution of Al by Zr are shown in Figure 25. Periodical sampling has shown that there is no crystalline material being formed in the first 12 days, but peaks appear in material that was sampled after 14 days. However, those are not characteristic peaks of UZM-9 zeolite, but rather

zeolite ZSM-39 of MTN framework since they correspond to diffractograms from reference[50]. Prolonging of synthesis up to 22 days results in more defined peaks, suggesting increase of crystallinity and decrease of amorphous phase, as visible by flatter baseline and higher intensities of peaks.

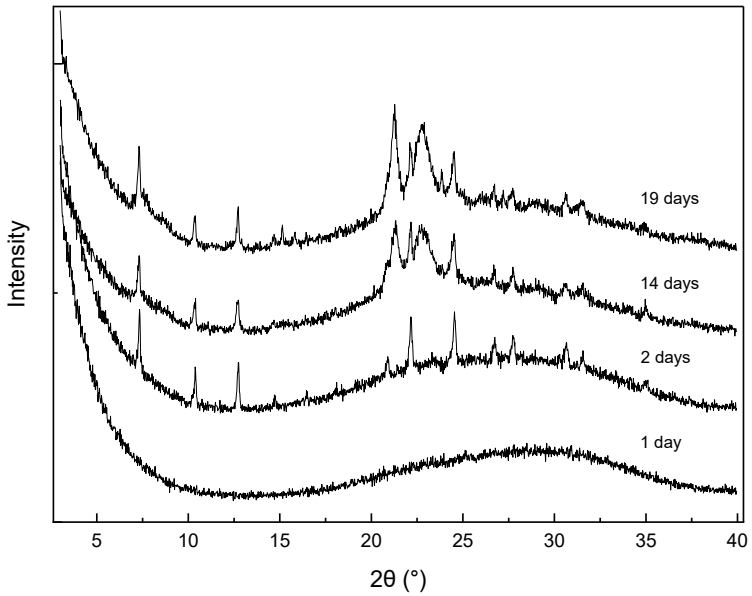

Figure 26: Diffractograms showing kinetics of crystallization from seeded synthesis with isomorphous substitution of Al by Zr

Kinetics from the synthesis of material prepared by isomorphous substitution of Al by Zr atoms, with an addition of UZM-9 seeding crystals, is shown in Figure 26. The presence of low-intensity peaks is visible already after 2 days of synthesis. However, those peaks have low intensities and periodic sampling had shown no changes until the fourteenth day of synthesis. The wide peaks between 20° and 23° appear only after fourteenth day and could be possibly explained by formation of some other crystalline material.

The synthesis with seeding results in Zr-UZM-9, however the background of its diffractogram is high and the intensities of the peaks in its diffractogram are very low, which could be possibly a result of small crystal sizes or difficult crystallization. On the other hand, the synthesis without seeding has diffractogram with lower background and more defined peaks. However, it produces different kind of material.

3.4. Experimental charge density matching approach

ECDM approach was explored as an alternative pathway to UZM-9 synthesis. Studying its effect on synthesis lengths, variance between used reactants and their effect on the final product, while being synthesised at temperatures lower than the ones from refference[18]

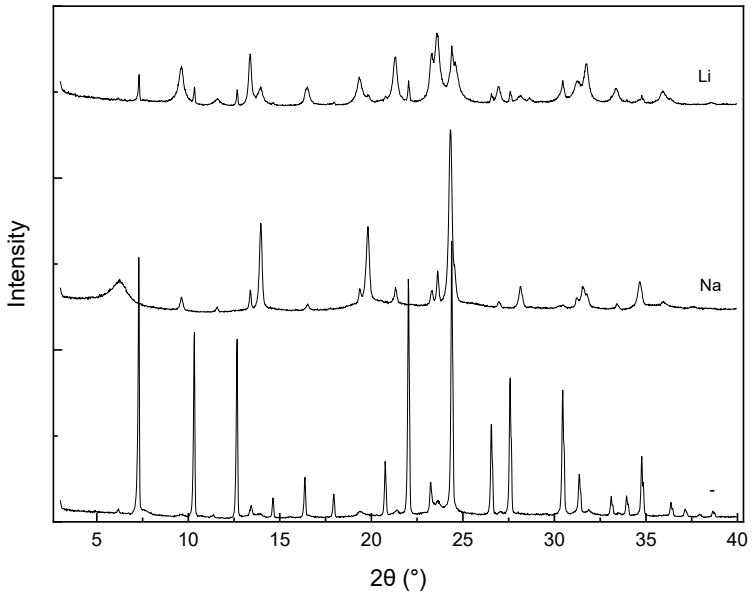

Figure 27: Diffractogram of materials prepared by ECDM approach to synthesis of zeolites after 13 days

Diffractograms in Figure 27 show that full crystallinity was not achieved in any of the prepared mixtures, even after 13 days, as it is visible by lack of flat baselines and presence of broad peaks. While the diffraction line of product from synthesis without addition of Li^+ or Na^+ cations shows the product closest to UZM-9 prepared in other syntheses, there are still many additional peaks, not present in diffractogram from patent[18] or the IZA database[19]. The other two syntheses show even worse results, with much broader peaks, at angles not corresponding to UZM-9 zeolite. This is most obvious in material with the presence of Na^+, indicating that UZM-9 was not formed. The material formed by synthesis with presence of Li^+ has the least defined peaks, with many of them broad and overlapping. However, some of their positions correspond to ones from successful syntheses, suggesting possibility of successfully replicating of this synthesis pathway. The overall length, difficulty of synthesis, and lack of desired products led to decision not to proceed with further exploration of ECDM approach. Further optimisation will be needed to get the UZM-9 zeolite, if possible.

4 Conclusions

UZM-9 zeolite was successfully prepared by hydrothermal synthesis. The optimization of the synthesis was successful, with the shortening of the synthesis length, by addition of seeding crystals. Furthermore, the amounts of seeding crystals were decreased down to 0.25 % of the synthesis mixture weight, with no effect on the synthesis length or quality of crystals, suggesting possibility of further decrease. Lowering the temperature from 150 to 125 °C as well as lowering of the amounts of SDA yielded negative results, with the prolonged synthesis time, making it infeasible. It was found that source of silica has an impact in preparation of synthesis mixture, with use of precipitated silica leading to easily mixed and homogenized gel. On the other hand, the untreated fumed silica results in dense mixture, that is difficult to homogenize.

The results of direct synthesis of Fe form of UZM-9 zeolite yielded negative results for syntheses with and without seeding, as it did not produce any crystalline material even after 19 days. On the other hand, direct synthesis of Zr form of UZM-9 zeolite led to formation of crystalline products. Seeded synthesis produced zeolite UZM-9 already after 2 days, although the diffractograms showed only low intensities of peaks and upon further synthesis led to formation of different and unknown material. Synthesis without seeding led to formation of ZSM-39 zeolite after 14 days of synthesis.

Adsorption studies were conducted on UZM-9 zeolites using nitrogen and carbon dioxide. Nitrogen adsorption yielded results that exceeded those from reference[18]. Seeding of syntheses also affected the adsorption properties, with much better results observed for seeded synthesis. Various ion-exchanged forms were investigated, demonstrating a dependence of adsorption on cation sizes, with Na-UZM-9 exhibiting better properties than Li-UZM-9. However, K-UZM-9 showed significantly lower values for BET, micropore, and total pore volume, possibly due to the large K^+ cations blocking the small pore openings. The CO_2 adsorption isotherms were utilized to calculate the isosteric adsorption heats of the prepared and ion-exchanged forms of the UZM-9 zeolite, with the calculated values decreasing as cation sizes increased.

Possibilities of large-scale synthesis as well as CH_4 adsorption studies are planned for further research of UZM-9 zeolite.

References

(1) Guo, P.; Wan, W.; McCusker, L.; Baerlocher, C.; Zou, X. On the Relationship between Unit Cells and Channel Systems in High Silica Zeolites with the “Butterfly” Projection. *Zeitschrift fur Kristallographie - Crystalline Materials* **2015**, *230* (5), 301–309. https://doi.org/10.1515/ZKRI-2014-1821.

(2) Anurova, N. A.; Blatov, V. A.; Ilyushin, G. D.; Proserpio, D. M. Natural Tilings for Zeolite-Type Frameworks. *Journal of Physical Chemistry C* **2010**, *114* (22), 10160–10170. https://doi.org/10.1021/JP1030027.

(3) Meier, W. M.; Moeck, H. J. The Topology of Three-Dimensional 4-Connected Nets: Classification of Zeolite Framework Types Using Coordination Sequences. *Journal of Solid State Chemistry* **1979**, *27* (3), 349–355. https://doi.org/10.1016/0022-4596(79)90177-4.

(4) Claire-Deville, H. de S. Reproduction de La Levyne. *Comptes Rendus* **1862**, *54*, 324–327.

(5) Ribeiro Ramoa, F.; Rodrigues, A. E.; Rollman, L. D.; Naccache, C. *Zeolites: Science and Technology*; Springer Netherlands, **1984**. https://doi.org/10.1007/978-94-009-6128-9.

(6) Barrer, R. M.; Denny, P. J. 201. Hydrothermal Chemistry of the Silicates. Part IX. Nitrogenous Aluminosilicates. *Journal of the Chemical Society (Resumed)* **1961**, *0* (0), 971–982. https://doi.org/10.1039/JR9610000971.

(7) *Framework Type codes*. https://www.iza-structure.org/.

(8) Zeolite Science and Perspectives. In *Zeolites in catalysis : Properties and Applications*; Čejka, J., Morris, R. E., Nachtigall, P., Eds.; The Royal Society of Chemistry, **2017**; pp 1–36. https://doi.org/https://doi.org/10.1039/9781788010610.

(9) Cesario, M. Romolos.; Macedo, D. A. de. *Heterogeneous Catalysis Materials and Applications*; Elsevier, **2022**. https://doi.org/https://doi.org/10.1016/C2020-0-02525-9.

(10) Mafra, L.; Vidal-Moya, J. A.; Blasco, T. Structural Characterization of Zeolites by Advanced Solid State NMR Spectroscopic Methods. *Annual Reports on NMR Spectroscopy* **2012**, *77*, 259–351. https://doi.org/10.1016/B978-0-12-397020-6.00004-0.

(11) Rasouli, M.; Yaghobi, N.; Chitsazan, S.; Sayyar, M. H. Influence of Monovalent Cations Ion-Exchange on Zeolite ZSM-5 in Separation of Para-Xylene from Xylene Mixture. *Microporous and Mesoporous Materials* **2012**, *150* (1), 47–54. https://doi.org/10.1016/J.MICROMESO.2011.09.013.

(12) Liu, C.; Xin, M.; Zhang, X.; Wang, C.; Qiu, L.; Xu, G. Unraveling the Separation Mechanisms of the LTA Zeolite Depending on the Regulated Particle Size and Pore Structure for Efficient Ethylene/Ethane Separation. *New Journal of Chemistry* **2023**, *47* (26), 12279–12286. https://doi.org/10.1039/D3NJ01217D.

(13) Wu, Y.; Weckhuysen, B. M. Separation and Purification of Hydrocarbons with Porous Materials. *Angewandte Chemie International Edition* **2021**, *60* (35), 18930–18949. https://doi.org/10.1002/ANIE.202104318.

(14) Zeolite Structures. In *Zeolites in catalysis : Properties and Applications*; Čejka, J., Morris, R. E., Nachtigall, P., Eds.; The Royal Society of Chemistry, **2017**; pp 37–72. https://doi.org/https://doi.org/10.1039/9781788010610.

(15) McCusker, L. B.; Baerlocher, C. Zeolite Structures. *Studies in Surface Science and Catalysis* **2005**, *157*, 41–64. https://doi.org/10.1016/S0167-2991(05)80005-9.

(16) *https://europe.iza-structure.org/IZA-SC/SBUList.html*.

(17) Mortier, W. J. (Wilfried J.); International Zeolite Association. Structure Commission. *Compilation of Extra Framework Sites in Zeolites*; Butterworth Scientific Limited on behalf of the Structure Commission of the International Zeolite Association, **1982**.

(18) Moscoso, J. G.; Lewis, G. J.; Gisselquist, J. L.; Miller, M. A.; Rohde, L. M. WO2003068679A1, **2003**. https://patents.google.com/patent/WO2003068679A1/en.

(19) *LTA: Framework Type*. https://asia.iza-structure.org/IZA-SC/framework.php?STC=LTA.

(20) Gómez-Hortigüela, L. *Insights into the Chemistry of Organic Structure-Directing Agents in the Synthesis of Zeolitic Materials*; **2018**. https://doi.org/https://doi.org/10.1007/978-3-319-74289-2.

(21) Kubota, Y.; Helmkamp, M. M.; Zones, S. I.; Davis, M. E. Properties of Organic Cations That Lead to the Structure-Direction of High-Silica Molecular Sieves. *Microporous Materials* **1996**, *6* (4), 213–229. https://doi.org/10.1016/0927-6513(96)00002-8.

(22) Synthesis of Zeolites. In *Zeolites in catalysis : Properties and Applications*; Čejka, J., Morris, R. E., Nachtigall, P., Eds.; The Royal Society of Chemistry, **2017**; pp 73–102. https://doi.org/https://doi.org/10.1039/9781788010610.

(23) Han, B.; Lee, S.-H.; Shin, C.-H.; Cox, P. A.; Hong, S. B. Zeolite Synthesis Using Flexible Diquaternary Alkylammonium Ions (CnH2n+1)2HN+(CH2)5N+H(CnH2n+1)2 with n) 1-5 as Structure-Directing Agents. *Chemistry of Materials* **2005**. https://doi.org/10.1021/CM048418.

(24) Hong, S. B. Use of Flexible Diquaternary Structure-Directing Agents in Zeolite Synthesis: Discovery of Zeolites TNU-9 and TNU-10 and Their Catalytic Properties. *Catalysis Surveys from Asia* **2008**, *12* (2), 131–144. https://doi.org/10.1007/s10563-008-9045-5.

(25) Lewis, G. J.; Miller, M. A.; Moscoso, J. G.; Wilson, B. A.; Knight, L. M.; Wilson, S. T. Experimental Charge Density Matching Approach to Zeolite Synthesis. **2004**, 364–372. https://doi.org/10.1016/S0167-2991(04)80824-3.

(26) Čejka, J.; Morris, R. E.; Nachtigall, P. *Zeolites in Catalysis : Properties and Applications*; **2017**. https://doi.org/https://doi.org/10.1039/9781788010610-00001.

(27) Khalid, S. X-ray Diffraction. In *Practical Guide to Materials Characterization*; Wiley, **2022**; pp 15–42. https://doi.org/10.1002/9783527838820.CH2.

(28) Byrn, S. R.; Zografi, G.; Chen, X. (Sean). X-ray Powder Diffraction. In *Solid State Properties of Pharmaceutical Materials*; Wiley, **2017**; pp 107–123. https://doi.org/10.1002/9781119264408.CH9.

(29) E. Wachs, I. Scanning Electron Microscopy (SEM). In *Characterization of catalityc materials*; E. Wachs, I., Ed.; Materials characterization series; CRC Press, **2010**.

(30) Thommes, M.; Kaneko, K.; Neimark, A. V.; Olivier, J. P.; Rodriguez-Reinoso, F.; Rouquerol, J.; Sing, K. S. W. *Physisorption of Gases, with Special Reference to the Evaluation of Surface Area and Pore Size Distribution (IUPAC Technical Report)*; Walter de Gruyter GmbH, **2015**; Vol. 87. https://doi.org/10.1515/PAC-2014-1117.

(31) Langmuir, I. The Constitution and Fundamental Properties of Solids and Liquids. Part I. Solids. *J Am Chem Soc* **1916**, *38* (11), 2221–2295. https://doi.org/https://doi.org/10.1021/ja02268a002.

(32) Sing, K. S. W.; Everett, D. H.; Haul, R. A. W.; Moscou, L.; Pierotti, R. A.; Rouquerol, J.; Siemieniewska, T. Reporting Physisorption Data for Gas/Solid Systems with Special Reference to the Determination of Surface Area and Porosity (Recommendations 1984). *Pure and Applied Chemistry* **1985**, *57* (4), 603–619. https://doi.org/10.1351/PAC198557040603.

(33) Thommes, M.; Kaneko, K.; Neimark, A. V; Olivier, J. P.; Rodriguez-Reinoso, F.; Rouquerol, J.; Sing, K. S. W. *IUPAC Technical Report Physisorption of Gases, with Special Reference to the Evaluation of Surface Area and Pore Size Distribution (IUPAC Technical Report)*; **2015**. https://doi.org/10.1515/pac-2014-1117.

(34) Brunauer, S.; Emmett, P. H.; Teller, E. Adsorption of Gases in Multimolecular Layers. *Journal of the American Chemical Society* **1938**, *60* (2), 309–319. https://doi.org/https://doi.org/10.1021/ja01269a023.

(35) Stepanov, A. G. Basics of Solid-State NMR for Application in Zeolite Science: Material and Reaction Characterization. In *Zeolites and Zeolite-like Materials*; Elsevier Inc., **2016**; pp 137–188. https://doi.org/10.1016/B978-0-444-63506-8.00004-5.

(36) Xu, J.; Wang, Q.; Li, S.; Deng, F. *Solid-State NMR in Zeolite Catalysis*; **2019**. https://doi.org/https://doi.org/10.1093/nsr/nwac155.

(37) Structure Determination. In *Zeolites in catalysis : Properties and Applications*; Čejka, J., Morris, R. E., Nachtigall, P., Eds.; The Royal Society of Chemistry, **2017**; pp 194–239. https://doi.org/https://doi.org/10.1039/9781788010610-00001.

(38) Parry, E. P. An Infrared Study of Pyridine Adsorbed on Acidic Solids. Characterization of Surface Acidity. *Journal of Catalysis* **1963**, *2* (5), 371–379. https://doi.org/10.1016/0021-9517(63)90102-7.

(39) Coelho, T. L.; Marinho, B.; Albuquerque, E. M.; Fraga, M. A. Discussing the Performance of Beta Zeolites in Aqueous-Phase Valorization of Xylose. *Catalysis Science & Technology* **2020**, *10* (21), 7165–7176. https://doi.org/10.1039/D0CY01176B.

(40) Wilschefski, S. C.; Baxter, M. R. Inductively Coupled Plasma Mass Spectrometry: Introduction to Analytical Aspects. *The Clinical Biochemist Reviews* **2019**, *40* (3), 115. https://doi.org/10.33176/AACB-19-00024.

(41) Kim, S. H.; Park, M. B.; Min, H.-K.; Hong, S. B. Zeolite Synthesis in the Tetraethylammonium–Tetramethylammonium Mixed-Organic Additive System. *Microporous and Mesoporous Materials* **2009**, *123* (1–3), 160–168. https://doi.org/10.1016/j.micromeso.2009.03.039.

(42) Rouquerol, J.; Rouquerol, F.; Llewellyn, P.; Maurin, G.; Sing, K. S. W. *Adsorption by Powders and Porous Solids: Principles, Methodology and Applications: Second Edition*; Academic Press, **2014**. https://doi.org/10.1016/C2010-0-66232-8.

(43) Lowell, S.; Shields, J. E.; Thomas, M. A.; Thommes, M. *Characterization of Porous Solids and Powders: Surface Area, Pore Size and Density*; Particle Technology Series; Springer, **2004**; Vol. 16. https://doi.org/10.1007/978-1-4020-2303-3.

(44) Lippens, B. C.; de Boer, J. H. Studies on Pore Systems in Catalysts: V. The t Method. *Journal of Catalysis* **1965**, *4* (3), 319–323. https://doi.org/10.1016/0021-9517(65)90307-6.

(45) JNM-ECZR Series NMR Spectrometer Z. JEOL Ltd. https://jeolusa.s3.amazonaws.com/resources_ai/jnmeczr_e_03.pdf?AWSAccessKeyId=AKIAQJOI4KIAZPDULHNL&Expires=2145934800&Signature=sDMqJl%2FHsh%2BpEb8%2BF5ujahrsm70%3D.

(46) Dědeček, J.; Tabor, E.; Sklenak, S. Tuning the Aluminum Distribution in Zeolites to Increase Their Performance in Acid-Catalyzed Reactions. *ChemSusChem* **2019**, *12* (3), 556–576. https://doi.org/10.1002/CSSC.201801959.

(47) Kubů, M.; Opanasenko, M.; Vitvarová, D. Desilication of SSZ-33 Zeolite – Post-Synthesis Modification of Textural and Acidic Properties. *Catalysis Today* **2015**, *243* (C), 46–52. https://doi.org/10.1016/J.CATTOD.2014.07.046.

(48) Kentish, S. E.; Scholes, C. A.; Stevens, G. W. Carbon Dioxide Separation through Polymeric Membrane Systems for Flue Gas Applications. *Recent Patents on Chemical Engineering* **2010**, *1* (1), 52–66. https://doi.org/10.2174/2211334710801010052.

(49) Zukal, A.; Pawlesa, J.; Čejka, J. Isosteric Heats of Adsorption of Carbon Dioxide on Zeolite MCM-22 Modified by Alkali Metal Cations. *Adsorption* **2009**, *15* (3), 264–270. https://doi.org/https://doi.org/10.1007/s10450-009-9178-5.

(50) *MTN: XPD Plot (verified syntheses)*. https://europe.iza-structure.org/IZA-SC/pow_plot_VerifSyn.php?STC=MTN&Syn_ID=58

(51) B. Wichterlová, Z. Tvarůžková, Z. Sobalík, P. Sarv, Determination and properties of acid sites in H-ferrierite: A comparison of ferrierite and MFI structures, *Microporous and Mesoporous Materials*, Volume 24, Issues 4–6, **1998**, Pages 223-233, https://doi.org/10.1016/S1387-1811(98)00167-X